THESIS FOR THE DEGREE OF DOCTOR OF PHILOSOPHY

Combination of space-geodetic techniques in the era of VGOS and multi-GNSS

PERIKLIS-KONSTANTINOS DIAMANTIDIS

Department of Space, Earth and Environment
Onsala Space Observatory
CHALMERS UNIVERSITY OF TECHNOLOGY
Gothenburg, Sweden 2023

Combination of space-geodetic techniques in the era of VGOS and multi-GNSS
PERIKLIS-KONSTANTINOS DIAMANTIDIS
ISBN 978-91-7905-817-3

ISSN 0346-718X
Department of Space, Earth and Environment
Onsala Space Observatory
Chalmers University of Technology
SE-412 96 Gothenburg
Sweden
Telephone: +46 (0)31-772 1000

Chalmers Reproservice
Gothenburg, Sweden 2023

Combination of space-geodetic techniques in the era of VGOS and multi-GNSS
PERIKLIS-KONSTANTINOS DIAMANTIDIS
Department of Space, Earth and Environment
Chalmers University of Technology

Abstract

The definition and maintenance of accurate and stable Earth-fixed and inertial reference frames is crucial in studying, among else, geophysical and geodynamical phenomena, precise positioning, and space navigation. The tools used to this end are space-geodetic techniques, like e.g., Very Long Baseline Interferometry (VLBI) and Global Navigation Satellite Systems (GNSS) which utilize signals from extraterrestrial radio sources to determine parameters of interest. An important concept in this regard is that of co-location. Stations of different space-geodetic techniques that are in close vicinity can be linked to the same frequency standards, are subject to similar loading effects, and share common atmosphere. In practice, they are also linked with observations that determine the vector between their respective reference points. These common features and inter-technique observations allow for the stacking of the heterogeneous space-geodetic observables in an estimation process that has been shown to suppress technique-specific biases and improve the accuracy and precision of the inferred parameters. The combination of space-geodetic techniques at co-location sites is delivering high-quality geodetic products. Recent developments in GNSS and VLBI include the incorporation of state-of-the-art instrumentation, in the form of satellite constellations in so-called multi-GNSS, or next-generation radio telescopes in VLBI that comprise the VLBI Global Observing System (VGOS). This thesis presents the principles of VLBI and GNSS, and then studies the untapped potential of novel concepts for the combination of space-geodetic techniques in the era of VGOS and multi-GNSS.

Keywords: GNSS, VLBI, Combination on the Observation Level, Space Geodesy, Local Ties, Reference Systems, EOP, multi-GNSS, VGOS

Acknowledgements

I would like to thank my supervisor Prof. Rüdiger Haas for the opportunity he has given me to work on this topic. I would also like to thank my co-supervisor Dr. Karine Le Bail for her support and belief in me. I had a happy working relationship with my colleagues over the years Niko, Joakim, Yiting, Rebekka, and Uttama. A special mention goes towards Dr. Grzegorz Kłopotek, for an excellent cooperation during the first 2.5 years of my PhD, and Prof. Thomas Hobiger for helping me to get started. I would also like to thank the senior staff of our group, Jan, Eskil, Maxime, and Gunnar who I also cooperated with in publishing my research.

The people from the department were kind and welcoming. The astronomers whom I considered a bit snobbish and abstract before coming here, have totally challenged preconceptions. Sandra, Daria, Andri, Flora, Kyoko and all the others. I met friends within the division, but also Chalmers in general. Francesco, Franz and Ioli I am looking at you. Not staring, just looking. I would also like to give a shoutout to Jessica, for putting up with me in the last and more challenging stage of my journey. Finally, I would like to thank my family for being close despite being far.

Publications

This thesis is based on the work contained in the following papers:

I P.-K. Diamantidis et al. (2021). VLBI and GPS inter-and intra-technique combinations on the observation level for evaluation of TRF and EOP. *Earth, Planets and Space*, **73**(1), 1–16. DOI: 10.1186/s40623-021-01389-1

II P.-K. Diamantidis et al. (2022). Combining VGOS, legacy S/X and GNSS for the determination of UT1. *Journal of Geodesy*, **96**(8), 55. DOI: 10.1007/s00190-022-01648-3

III P.-K. Diamantidis and R. Haas (2022). Evaluation of the first three years of VGOS 24 h sessions using a kalman filter with c5++. *Earth, Planets and Space*. in review

IV P.-K. Diamantidis et al. (2023). On the possibility of site-based combinations using a single point. *Journal of Geodesy*. in review

V G. Elgered et al. (2023). Assessment of GNSS stations using atmospheric horizontal gradients and microwave radiometry. *Advances in Space Research*. in review

Other research contributions not included in the thesis:

G. Elgered et al. (2022). Comparison of four different GNSS antenna installations using estimated atmospheric gradients and microwave radiometry. *Proceedings of the 8th International Colloquium on Scientific and Fundamental Aspects of GNSS*.

R. Haas et al. (2023). Assessment of Parameters Describing the Signal Delay in the Neutral Atmosphere Derived from VGOS Observations. *IVS 2022 General Meeting Proceedings*, 248–252, Edited by Kyla L. Armstrong, Dirk Behrend, and Karen D. Baver, **N**ASA/CP-20220018789

Contents

Chapter 1
Introduction

> Hesiod scratched his beard. Back in those days, you couldn't be a wise person, unless you had a beard. Nowadays, if you do have one, you are either a tourist, a poet or a fool. But in those times, the electric trimmer hadn't been invented yet, so beards were common. Hesiod, scratched his beard, and wrote:
>
> "In the beginning, there was Chaos."
>
> Chaos is always around us. In politics. In these mysterious murders where bullets fly through a window and pierce a piece of Chaos. In the big trusts but also in the lives of the common people who just try to make ends meet. Chaos created us, and it relentlessly strives to turn us back into its fold. Chaos, this viscous, dark, watery, mysterious and unknown substance. If we ever knew what it was, we would be Gods. Better we never do!
>
> Hesiod claimed it was Space. Damn him and his writings! But since he said so, we say so. And Space had inside it, in sperm form, the Universe.
>
> (Tsiforos, 1975)

The human condition is inextricably intertwined with the attempt to describe and define Chaos. If Chaos can be thought of as Space, measuring it is essential to defining and understanding it. Nikos Tsiforos, as stated in the above excerpt, disapproves of such an endeavor; not because of its futility, but because of the fact that knowledge relates to power in a dynamic that can become extremely volatile. A postmodernist view would attempt to reject the notion of a universal definition of the world, be it Chaos, Space or the Universe. The metrological sciences are, in contrast, on the other end of this spectrum. Instead of theorizing about the existence of Space, or viewing it from an ideological perspective, they pragmatically study it. When this study develops into tools and methods to define and describe Earth within Space, the scientific field it belongs to is called Space Geodesy.

The necessity for precise definitions of terrestrial and celestial reference frames and the determination of parameters that describe the Earth's orientation in inertial

space, so-called Earth Orientation Parameters (EOP) are central to this field. In order to achieve this goal, different space-geodetic techniques were developed, i.e., techniques that rely on signals from extraterrestrial sources to infer frame definitions and EOP. These techniques include Very Long Baseline Interferometry (VLBI), Global Navigation Satellite Systems (GNSS), Satellite Laser Ranging (SLR), Lunar Laser Ranging (LLR) and Doppler Orbitography and Radiopositioning Integrated by Satellite (DORIS). When used independently, they suffer from technique-specific systematic errors and, apart from VLBI, are limited in the EOP that they are sensitive to. The active suppression of said errors can be partially achieved by improved modelling and equipment but in a metrological sense it can only ultimately come from the diversification of information that infer parameters of interest. In other words, the meaningful combination of said techniques holds the promise of ever more precise determinations.

In this context, the International Earth Rotation and Reference Systems Service (IERS) has established and operated working groups towards examining different methods of rigorous combination of space-geodetic techniques (Gambis et al., 2012). In parallel the concept of fundamental stations, i.e., sites that are able to record observations from multiple space-geodetic techniques, has risen in prominence given the potential that simultaneity and temporal correlation gives between different observables.

1.1 Outline of the thesis

This thesis delves deeper into the topic of different methods to achieve combination of multiple space-geodetic techniques. In particular, Chapter 2 gives an introduction into the common framework which is present in all space-geodetic techniques, namely spatio-temporal reference frames and common parameters of interest that are estimated during data analysis. Chapters 3 and 4 present basic concepts of GNSS and VLBI, respectively, that need to be taken into account during the estimation and/or combination process and their contributions to space-geodetic products. Different combination schemes are analysed in Chapter 5, and all the paper contributions of this thesis are presented. Finally, Chapter 6 provides a summary of each paper and a general outlook.

Chapter 2

Space Geodesy

Space-geodetic techniques share a common mode of operation. Earth-based stations collect and time-tag signals, coming either from an extra-galactic source, an artificial satellite or the Moon. The stations, positioned on the Earth's crust, are affected by a plethora of geodynamical phenomena that perturb their position. The signals experience some form of refraction when propagating through the atmosphere which distorts their path. The collected data are processed with the aim of aiding in the establishment of stable reference frames. A description of the reference systems and frames as well as error sources common to most techniques that occur during this signal propagation and acquisition process follows.

2.1 Reference Systems

The definition, realisation and maintenance of reliable reference systems is essential for space-geodetic applications that rely on the utmost precision, in order to quantify, separate and study different geodynamical phenomena and parameters of interest. While reference systems are the theoretical framework consisting of the goals, conventions and formalisations used, the actual realisation comes in the form of reference frames. These frames consist of a robust catalogue of coordinates of well-defined points, which enable users to gain access to high quality geodetic products.

To fulfill this goal, both Earth-fixed and inertial reference systems and frames have been developed. One of the well-established Earth-fixed or terrestrial reference systems is the so-called International Terrestrial Reference System (ITRS). The ITRS is realised as the International Terrestrial Reference Frame (ITRF) through the determination of zeroth and first time-derivatives of its origin, orientation and scale. The ITRF is maintained and routinely updated by the IERS, with the latest version designated as the ITRF2014 (Altamimi et al., 2016). The International Celestial Reference System (ICRS) is the counterpart of ITRS in the inertial space. Its origin is at the barycenter of the solar system although an equivalent system with a different origin definition, that of the geocenter, is also used, the Geocentric Celestial Reference System (GCRS). The realisation of the ICRS is predominantly

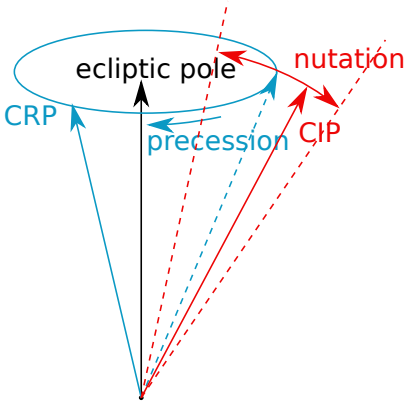

(a) *The nutation/precession movement along with the Celestial Intermediate Pole (CIP) to Celestial Reference Pole (CRP) transformation. Notice that the effect of nutation is exaggerated for illustration purposes.*

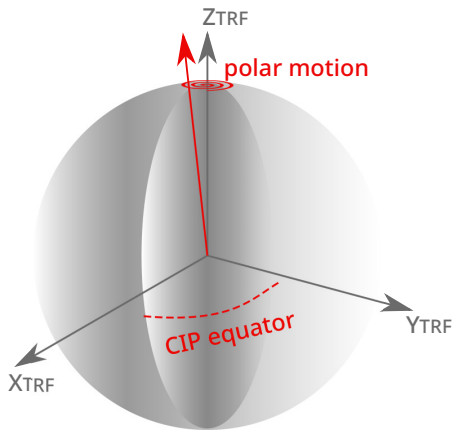

(b) *The polar motion and the Terrestrial Reference Frame (TRF) axes.*

Figure 2.1: *Representations of the nutation/precession in (a) and polar motion in (b).*

used by the International Astronomical Union (IAU) and maintained by the IERS in the form of the International Celestial Reference Frame (ICRF) with its latest version, the ICRF3 (Charlot et al., 2020).

The Earth's motion can be described as an axis-angle rotation where the axis of rotation itself is changing orientation. This change is the superimposition of rotational movements with different periodicities, a key feature that allows for their separation and study (Petit and Luzum, 2010). In particular, the orientation of the rotation axis is changing with respect to the Earth's crust, a phenomenon which is called polar motion (PM). Earth's rotation axis also shows an obliquity, i.e., an axial tilt, with respect to its orbital plane around the sun, i.e., the ecliptic plane. This tilt is not constant but shows a small variation over time, described by nutation. The rotation axis, retrieved by the mean obliquity, is in turn rotating with respect to the ecliptic pole, a phenomenon called precession. Figs. 2.1a- 2.1b show the nutation/precession effect separately, i.e., the trace of the combined movement of the CIP is not visible, as well as polar motion.

The rotation axis is always perpendicular to the equatorial plane of a reference system. The origin of the longitude in the equatorial plane of the Earth-fixed system known as the Terrestrial Intermediate Origin (TIO) is rotating with respect to the origin of the right ascension of the Celestial Intermediate Pole (CIP) equator, so-called Celestial Intermediate Origin (CIO). The angle that is formed between them is called Earth Rotation Angle (ERA). Space-geodetic techniques can be used for determining corrections on the precession/nutation model (also called

celestial pole offsets, dX, dY), the x- and y-component of the polar motion (x_p, y_p), and the ERA, or the equivalent concept of Universal Time ($UT1$). This completes the axis-angle description of the motion of the Earth, and the set of these five parameters constitute the EOP.

The transformation procedure between the GCRS and the ITRS is as follows (Petit and Luzum, 2010)

$$\vec{X}_{GCRS} = Q(t)R(t)W(t)\vec{X}_{ITRS}, \tag{2.1}$$

where $Q(t)$ is the composite rotation matrix for precession/nutation, $R(t)$ the rotation matrix for Earth rotation and $W(t)$ the one for polar motion. As Eq. 2.1 shows, the transformation between the two reference systems is reminiscent of the procedure normally applied to the transition between orbital planes of common origin, eccentricity and size of semi-major axis. Three elemental rotations are used around the two of the three axes attached to the orbital plane, with angles (a) u_0 or argument of the latitude, (b) i or inclination and (c) Ω or right ascension of the ascending node.

2.2 Time Systems

Space Geodesy is based on recording the time of arrival of signals, either from or to a satellite or another extraterrestrial source and their subsequent correlation in order to extract a time-delay. As important as it is to define a precise reference frame in the confines of the three-dimensional space, the same is equally true to time. The concept of hour angle finds widespread use in this context. Hour angle is the angle between the local meridian and the path pointing to the vernal equinox, i.e., the CIO.

2.2.1 Sidereal and Universal Time

The transformation of the hour angle in time units, provides the so-called sidereal time. This time definition suffers from both irregularities in Earth's rotation but also from the effects that precession and nutation have on the CIP equator. The concept of a "true" vernal equinox, which materialises after removing the bias induced by the precession effect gives what is known as the Local Apparent Sidereal Time (LAST). Correcting for both precession/nutation gives the "mean" vernal equinox and the so-called Local Mean Sidereal Time (LMST). If instead of the local meridian, the Greenwich meridian is used, LMST and LAST are converted to GMST and GAST where "G" stands for Greenwich. Tracing a "mean" Sun (since the true movement of the Sun is not uniform) instead of the CIO can be used, which enables the Universal Time (UT) to be retrieved. If the effect of the polar motion is removed the UT transforms to $UT1$. The $UT1$ parameter is linked to ERA through a linear relationship (Capitaine, 2008)

$$ERA(T_u) = 2\pi(0.7790572732640 + 1.00273781191135448T_u), \tag{2.2}$$

where T_u = (Julian $UT1$ date - 2451545.0).

2.2.2 Atomic Time

The state-of-the-art time scale which is used today is the Atomic Time (TAI - Temps Atomique International) which is maintained by the IERS and the Bureau International des Poids et Mesures (BIPM). The weighted average of a number of free-running atomic clocks is computed in the form of the Free Atomic Scale (EAL - Échelle Atomique Libre). This is then steered to maintain agreement with the SI definition of a second (Petit et al., 2015). The $UT1$ parameter is affected by the perturbations of the angular velocity of the Earth's rotation, meaning that there are discrepancies with respect to TAI. To keep track of these, the Coordinated Universal Time (UTC) has been introduced, which is a discretized approximation on the level of seconds of $UT1$ and has its basis on TAI, i.e.,

$$UTC = TAI + ls, \tag{2.3}$$

where ls are the leap seconds added, so that $UT1 - UTC$ is maintained in the sub-second level. When estimating EOP, instead of $UT1$, the $UT1 - UTC$ value is also used, along with the excess revolution time, or Length of Day (LOD).

2.3 Atmospheric Refraction

The distortion of the signal paths as they propagate through the atmosphere is a common error source in all microwave-based space-geodetic techniques. The physical phenomena that cause it are (a) the induced and permanent dipole moments of neutral atmospheric gases and water vapor respectively, resulting in what is commonly referred to as tropospheric delay, and (b) the dispersion due to the free electrons in the ionosphere, leading to the so-called ionospheric delay.

2.3.1 Tropospheric Delay

Any signal travelling through the neutral atmosphere experiences refraction which leads to an alteration of both of its path as shown in Fig. 2.2a and phase velocity. The layered atmosphere approximation can lead to determination of the signal path delay. The magnitude of the phase velocity at layer n, $v_{ph,n}$, can be retrieved from the refractive index n_n since by definition $n_n = \frac{c}{v_{ph,n}}$. The change of the signal path when it enters layer n can be determined by the ratio of the refractive indices through Snell's law, $\frac{sin\theta_{n+1}}{sin\theta_n} = \frac{n_n}{n_{n+1}}$, where θ is the angle measured from the normal of the boundary. Details are present in Fig. 2.2b. The time delay t_d of the arrival of the signal is $t_d = \int_S \frac{1}{v_{ph}(s)} ds - \int_G \frac{1}{c} dg$, which can be converted to path length as

$$\Delta L^T = \int_S (n(s) - 1) ds + S - G. \tag{2.4}$$

As we see in Eq. 2.4, the delay term ΔL^T takes into account the geometry of the two paths S and G, which constitutes the "geometric delay", and the divergence of the phase velocity in the atmosphere from the value it has in vacuum. Notice that

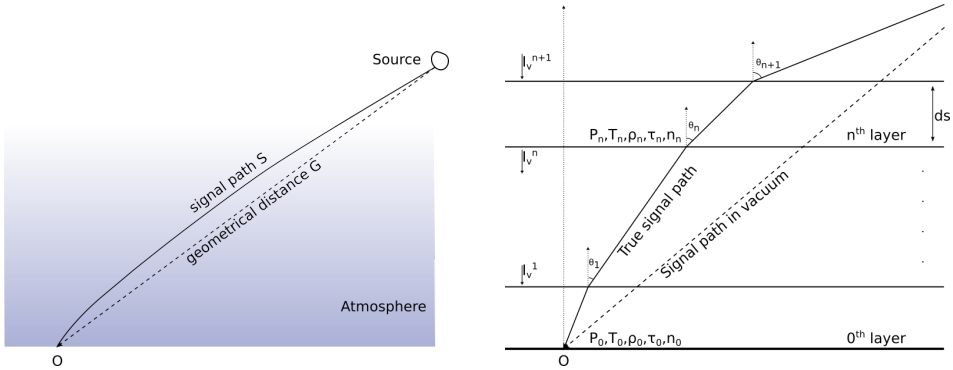

(a) *True, S, and geometrical, G, signal path.*

(b) *Ray tracing through a horizontally-stratified atmosphere.*

Figure 2.2: *The "bending" of the signal path due to the refraction in the atmosphere. Instead of following the geometrical path, G, the true signal path, S, is presented. Note that the effect is exaggerated for the purposes of illustration.*

$n(s) - 1$ in Eq. 2.4 can be alternatively written as $n(s) - n_{vacuum}$ as the refractive index in vacuum is equal to 1. It is also worth noting that through Snell's law, for a horizontally stratified atmosphere, a signal at zenith, i.e., with angle $\theta = 0$ will not experience refraction and thus paths S and G will be identical. In this case the so-called path delay at zenith, $\Delta L^{T,z}$, will be solely dependent on the change in phase velocity.

The path delay contains the accumulated effect of all atmospheric gases, the water vapor and the liquid water and can be split up into "dry" and "wet" parts, $\Delta L^T = \Delta L^T_{dry} + \Delta L^T_{wet}$ (Davis et al., 1985). The contribution of most of the "dry" atmospheric components can be concentrated in the first term and can be shown to be modelled well using measured total pressure at ground level. The wet term $\Delta L_{T\,wet}$ cannot be easily inferred due to poor correlation between water vapor density on the ground and at different altitudes. It becomes, therefore, an error source that must be estimated and removed from space-geodetic observables. The most prominent way of accomplishing this is by approximating it as a linear function of the "wet" delay at zenith, $\Delta L^T_{wet} = mf_w \Delta L^{T,z}_{wet}$ where the term mf_w is an elevation-dependent mapping function. The coefficients that may complement a mapping function can be a result of empirical data or global grid models (Boehm et al., 2006; Landskron and Böhm, 2018).

Another way of looking at tropospheric delay is by approximating the troposphere as an inverse cone with its tip at the receiver point, a radius of 65 km and a height of the tropopause between 9 km and 17 km (Walpersdorf et al., 2001). Mapping functions inflate the estimated delay at zenith with an elevation-dependent value. They are, therefore, insensitive to azimuthal variations. Signals that arrive in concentric rings per elevation angle are approximated as experiencing the same delay. The effect is visible in Fig. 2.3. A more sophisticated approach attempts to

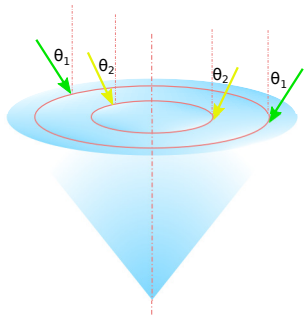

Figure 2.3: *For a homogeneous atmosphere all signals with the same angle of incidence experience the same delay irrespective of azimuthal direction. The difference in delay is thus only visible for groups of signals of different angles like, e.g., the green ones (angle θ_1) in contrast to the yellow ones (angle θ_2).*

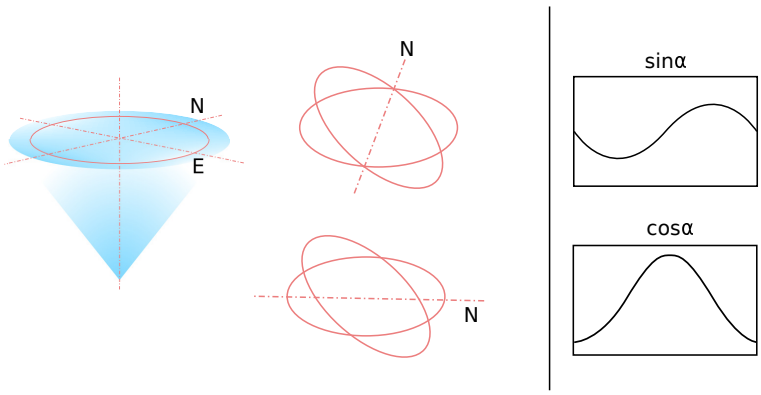

Figure 2.4: *For an inhomogeneous atmosphere there is an azimuthal variation of the troposphere delay, shown on the right, as a response to a rotation of the base plane of the cone around the north (top) and the east (bottom) axis.*

tilt the base of the inverted cone, denoting the presence of a gradient. As Fig. 2.4 shows, rotation around the north axis gives a variation of a sine pattern along the trace of the circle with the maximum/minimum occurring in the east/west direction, G_E, while a rotation around the east axis gives a cosine pattern with maximum/minimum in the north/south direction, G_N. One can thus augment the wet tropospheric delay by

$$\Delta L_{wet}^{T} = mf_w \Delta L_{wet}^{T,z} + mf_g(G_N \cos\alpha + G_E \sin\alpha), \tag{2.5}$$

where mf_g a gradient mapping function and α the azimuth angle.

2.3.2 Ionospheric Delay

The ionosphere is, as opposed to the troposphere, a dispersive medium. This means (a) that the phase velocity is frequency-dependent and (b) that the group and phase velocities are different. The latter can be inspected via the relation between the angular frequency ω and the wave number k, which is described as

$$\omega^2 = c^2k^2 + \omega_p^2, \tag{2.6}$$

where $\omega_p = 2\pi f_p$, $f_p = 8.98\sqrt{N}_e$ and N_e the electron density. Since phase velocity is $v_{ph} = \frac{\omega}{k}$ and group velocity is $v_{gr} = \frac{d\omega}{dk}$, they can only be equal if ω and k are directly proportional, something that Eq. 2.6 clearly violates. The magnitude and relation between group and phase ionospheric delays can be established (Petit and Luzum, 2010). In particular, they have inverse signs and equal magnitudes which for the case of the phase delay is

$$\Delta L_p^I(f) = -\frac{s_1}{f^2} - \frac{s_2}{f^2} - \frac{s_3}{f^2}, \tag{2.7}$$

where s_1, s_2 and s_3 are first second and third order terms. These are equal to (Petit and Luzum, 2010)

$$\begin{aligned} s_1 &= 40.309 \int_L N_e dl, \\ s_2 &= 1.1284 \cdot 10^{12} \int_L N_e B \cos\theta dl, \\ s_3 &= 812.42 \int_L N_e^2 dl + 1.5793 \cdot 10^{22} \int_L B^2(1+\cos\theta^2) dl, \end{aligned} \tag{2.8}$$

where B is the geomagnetic field modulus, θ the angle between the signal and the geomagnetic field. Integrating the electron density over the total path gives the Slant Total Electron Content

$$STEC = \int_L N_e dl, \tag{2.9}$$

which incorporated in the first-order term s_1 of Eq. 2.8 gives the phase ionospheric delay as

$$\Delta L_p^I(f) \approx -\frac{40.309}{f^2} STEC. \tag{2.10}$$

This is an approximation that neglects the higher-order terms which may need to be incorporated, depending on the application (Petit and Luzum, 2010). It is important to note that the total electron content (TEC) exhibits diurnal variations as the Sun affects the ionisation of the upper atmosphere, as well as the aforementioned frequency dependence of the ΔL_p^I (and also ΔL_g^I) as shown in Eq. 2.10. The main ways to mitigate ionospheric delay are (a) to observe at multiple frequencies and combine measurements so that the effect of the ionosphere is removed or (b) through the use of empirical models or space-geodetic observables to produce world grids of TEC the so-called vertical TEC (VTEC) maps. These are distributed in specialised data formats, an example of them being the Ionosphere map Exchange format (IONEX) (Hernández-Pajares et al., 2009). The first-order approximation removes most of the ionospheric effect but VTEC products also allow for the mitigation of the higher-order terms.

2.4 Displacements

Geodynamical phenomena that are triggered by either the gravitational attraction between Earth and other celestial bodies, or a direct result of the endogenic processes of the Earth itself, result in a variability of station coordinates over time. The motion can be decomposed in tidal and non-tidal effects. First-order tidal effects due to luni-solar attraction, also known as solid Earth tides (Agnew, 2015), and second-order effects like the elastic response of the Earth's crust to (a) ocean tides (ocean loading) (Scherneck and Webb, 1999), (b) the differential in atmospheric pressure with respect to time (atmospheric loading) (Boy et al., 1998), (c) the shift in Earth's axis of rotation (pole tide) (Miller and Wunsch, 1973). The combined effect can reach up to a level of tens of centimeters. Non-tidal components of the above are also present (Williams and Penna, 2011), as well as local variations maybe present like interseismic (Biggs et al., 2007) or postseismic deformations (Hearn et al., 2009) of the Earth's crust, which can significantly affect geodetic measurements (MacMillan et al., 2012).

Chapter 3

Global Navigation Satellite Systems

The principles of Global Navigation Satellite Systems (GNSS) were first demonstrated in the 1950's and early 1960's as a technique used for satellite tracking by measuring the frequency Doppler shift with respect to a ground station of known position. Equivalently in a reverse process, satellites that inhabit known orbits can be used to determine geodetic positioning of a ground station. This concept was explored by the TRANSIT system, the first such satellite system with global coverage (Kumar and Moore, 2002).

Modern GNSS, such as the Global Positioning System (GPS), rely on range measurements between their space-based segment, i.e., a satellite constellation, and the ground-based segment, i.e., receivers. The time of arrival (TOA) of a signal transmitted by a GPS satellite is determined at the receiver, allowing for a range to be estimated. Since range is a one-dimensional quantity and therefore lacks information about the direction of the transmitter, three measurements would be needed to establish the position of the receiver, in a process known as trilateration (Fig. 3.1). In reality, biases induced because of timing inconsistencies between transmitter and receiver clocks, mean that a fourth measurement needs to be added in order for the positioning of the receiver to be determined with reasonable accuracy, with more measurements contributing to the over-determination of the problem and thus increased accuracy.

While, as the name suggests, GNSS are used in the field of navigation, they have found multi-disciplinary use in, among others, satellite tracking, remote sensing and Space Geodesy (Jin et al., 2014; Prange et al., 2017; Springer et al., 2011). For the latter in particular, it is forming a part of the satellite geodesy branch. The establishing of permanently installed GNSS receivers in a dense worldwide network and the subsequent acquisition and analysis of GNSS data, has developed products that support the monitoring of Earth's rotation and polar motion and the study of geodynamical phenomena like, e.g., crustal deformation or tectonic plate movement (Brockmann et al., 2012; C. E. Noll, 2010). This activity mainly takes place through the International GNSS Service (IGS), an association of research institutes worldwide that voluntarily maintains and updates space-geodetic products (Johnston et al., 2017).

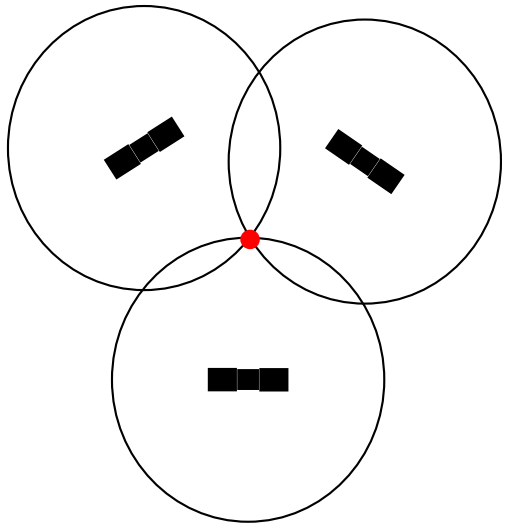

Figure 3.1: *Visualisation of the trilateration procedure for determination of a point in 2D space. The satellites (black) send out signals that are received at the receiver (red). By intersection of the circles the receiver's position is determined.*

The first fully operational GNSS was GPS, which is now complemented by several other systems that offer global coverage, namely, the Russian GLONASS, the European Galileo, and the Chinese Beidou. A multi-GNSS experiment (MGEX), has been initiated by IGS with the aim of exploring the new capabilities that the combination of different GNSS can offer (Montenbruck et al., 2017).

3.1 Basic GNSS Observables

Modern GNSS receivers determine the range between the transmitter and the receiver in two different ways.

- Firstly, by cross-correlating the incoming signal with a signal replica that the receiver produces using its own internal clock and acquiring the time of arrival (TOA), the so-called code-phase measurement.

- Secondly, by counting the total number of cycles that the carrier wave of the incoming signal has travelled, the so-called carrier-phase measurement.

Eqs 3.1-3.2 for code-phase, R_p, and carrier-phase, Φ_L, measurements show that both of them infer a slant range, ρ, with the rest being error sources that need to be estimated and removed. Notice that notation of instrumental delays and

multipath in carrier-phase is the lower-case equivalent of the code-phase.

$$R_P = \rho + \underbrace{c(dt_r - dt^s)}_{\text{clock bias}} + \overbrace{T}^{\text{troposphere}} + \underbrace{\alpha_f STEC}_{\text{ionosphere}} + \overbrace{K_{P,r} - K_{P^s}}^{\text{receiver \& satellite instrumental delays}} \tag{3.1}$$

$$+ \underbrace{M_P}_{\text{multipath}} + \overbrace{\epsilon_P}^{\text{random noise}}$$

$$\Phi_L = \rho + c(dt_r - dt^s) + T - \alpha_f STEC + k_{L,r} - k_{L^s} + \underbrace{\lambda_L N_L}_{\text{phase ambiguity}} + \overbrace{\lambda_L w}^{\text{phase windup}} \tag{3.2}$$

$$+ m_L + \overbrace{\varepsilon_L}^{\text{random noise}}$$

There are at least two frequencies on which GNSS transmitters emit signals. This allows for the existence of multiple carrier- and code-phase observables. Different linear combinations between two frequencies can be used to remove error sources. One example is the linear combination which eliminates the ionospheric delay

$$R_C = \frac{f_1^2 R_{P1} - f_2^2 R_{P2}}{f_1^2 - f_2^2} = \rho + c(\delta t_r - \delta t^s) + T + M_C + \epsilon_C, \tag{3.3}$$

$$\Phi_C = \frac{f_1^2 \Phi_{L1} - f_2^2 \Phi_{L2}}{f_1^2 - f_2^2} = \rho + c(\delta t_r - \delta t^s) + T + B_C + \lambda_N w + m_C + \varepsilon_C, \tag{3.4}$$

with $B_C = b_C + \lambda_N(N_1 + \frac{\lambda_W}{\lambda_2} N_W)$, where $\lambda_N = \frac{c}{f_1 + f_2}$, $\lambda_W = \frac{c}{f_1 - f_2}$ and $N_W = N_1 - N_2$. Note that terms containing the subscript C are $(\cdot)_C = \frac{f_1^2 (\cdot)_1 - f_2^2 (\cdot)_2}{f_1^2 - f_2^2}$. Further combination corroborates in the carrier-phase ambiguity resolution procedure.

Carrier-phase Ambiguity Resolution

Regarding carrier-phase measurements, the fractional phase difference between the incoming signal and the signal replica can be determined with great precision via the use of a numerically controlled oscillator in the receiver. The integer number of cycles, however, is an ambiguous term when a satellite first comes into view making the resolution of this ambiguity a necessary step in the estimation procedure.

As Eq. 3.2 shows, the main error sources are the tropospheric and ionospheric delay, the multipath and instrumental delays as well as the integer ambiguity term. Estimating or removing these error sources depends on whether one can gather quasi-independent information about them and formulate a properly defined estimation problem. The tropospheric delay, for example, which is dependent on the signal path, can be adequately defined at zenith, if there are visible satellites at different azimuth and elevation angles, i.e., at different paths. Equivalently,

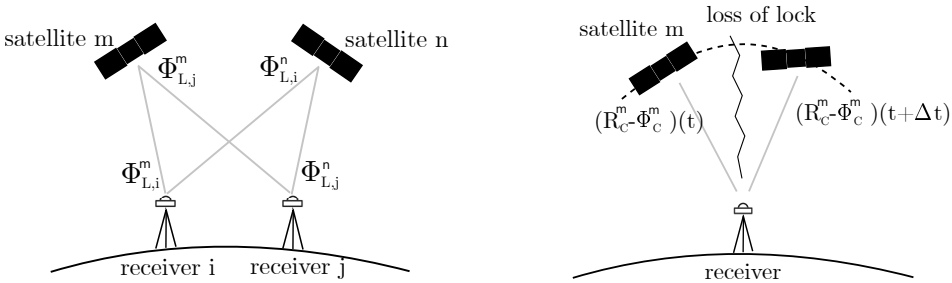

(a) *Double-differencing* (b) *Time-differencing*

Figure 3.2: *(a) The double-differencing (DD) technique is using two satellites and two receivers to allow determining integer ambiguities. (b) In time-differencng (TD) a single pair of satellite and receiver is used, determining float ambiguities. See text for further details.*

in order for the instrumental delays of satellites and receivers to be quantified, observables from multiple satellites and multiple receivers must be used. Linear combinations of that manner, through a process called double-differencing (DD) as shown in Fig. 3.2a, produce phase observables which are free of instrumental delays, making the determination of the integer ambiguity term possible. Indeed $\Phi^m_{L,ij} = \Phi^m_{L,i} - \Phi^m_{L,j}$ and $\Phi^n_{L,ij} = \Phi^n_{L,i} - \Phi^n_{L,j}$ have $k^m_{L,ij}$ and $k^n_{L,ij}$ as instrumental delays which represent approximately the same quantity and further differencing produces the desirable DD observable $\Phi^{mn}_{L,ij} = \Phi^m_{L,ij} - \Phi^n_{L,ij}$ free of these biases. Multiple procedures of retrieving the integer term based on this concept have been developed (Teunissen et al., 2002).

An alternate route would be to not attempt fixing the ambiguities at their physical integer value. Treating them as floats implicitly means two possibilities, either (a) the ambiguity term is not confined to the integer space in the estimation problem containing the DD observables, or (b) the estimation problem is not constructed using DD observables at all. The latter means that one can use the raw measurements or more commonly the ionosphere-free linear combination in the time-differencing procedure. Under this regime, as shown in Fig. 3.2b, the evolution of geometry-free linear combination, $R_C - \Phi_C$, is monitored, and discovered discrepancies between subsequent time epochs are quantified to determine the magnitude of the float ambiguity. The precise positioning determination of a single receiver can be achieved, using just its own data, without the need to resort to the interferometric nature of DD. The instrumental delays are not explicitly removed but instead they are incorporated in the float ambiguity term. This single-receiver estimation process is called Precise Point Positioning (PPP). Lately, there has been development in combining this technique with global solutions to derive integer ambiguities (Geng et al., 2010; Laurichesse et al., 2009).

3.2 Receiver Clock Treatment

The signal which is emitted from the satellite consists of a carrier wave, modulated by the navigation message and a spread-spectrum technique so that the final signal has a unique time-dependent form. The signal replica is produced at the receiver in a similar fashion. For the two signals to be perfectly aligned, it would mean that the internal clocks of the receiver and the satellite need to be perfectly synchronised, which is never the case. It is this discrepancy between internal time-keeping mechanisms of space-based and ground-based segments of the system that produces a relative clock bias, $(dt_r - dt^s)$, as Equation 3.1 shows. Notice that this term contains dt_r which corresponds to the difference between receiver-kept time and true time, and dt^s which corresponds to the difference of the satellite-kept time and true time. Information about dt^s can be found either in the navigation message or in precise timing products obtained directly by IGS. This in turn disentangles the two quantities and allows for the determination of dt_r, i.e., the clock stability of the receiver clock. It is thus evident that any imperfection in the definition of the satellite clock is reflected on the behavior and the definition of the receiver clock. This highlights the importance of acquiring high-quality clock products especially if the subsequent estimation procedure is dependent on approximating the behavior of the clock via a stochastic process, which demands adherence to strict clock definitions.

Another important realisation is that linear combinations alter said definitions. The ionosphere-free observable contains $\delta t = (\delta t_r - \delta t^s)$, which is an "ionosphere-free" clock term with potentially different stability characteristics than the one from the raw measurements. Clock terms can be further augmented with, e.g., the instrumental delays of satellites and receivers which, since they are different for code- and carrier-phase, result in a so-called decoupled clock model with separate code and phase clocks (Collins et al., 2008). Notice also that the receiver clock bias cannot be meaningfully estimated if its value is lower than the noise level of the measurements. For these reasons, one cannot expect different definitions of GNSS receiver clocks to consistently behave approximately the same as the nominal one. An example of different clock behaviors due to these effects is shown in Fig. 3.3. While the "ionospheric-free" clock is used in all of them, the stability characteristics vary, from being close to nominal clock stability of an H-maser, as seen for the Matera clock, to showing large discrepancies, as seen for the other three example clocks.

3.3 GNSS in Space Geodesy

Code- and carrier-phase observables as shown in eqs 3.1-3.2 contain a slant range parameter, ρ. This is equal to the euclidean norm of the vector between satellite and receiver positions, $\vec{p^s}$ and $\vec{p_r}$

$$\rho = \|\vec{p^s} - \vec{p_r}\|. \tag{3.5}$$

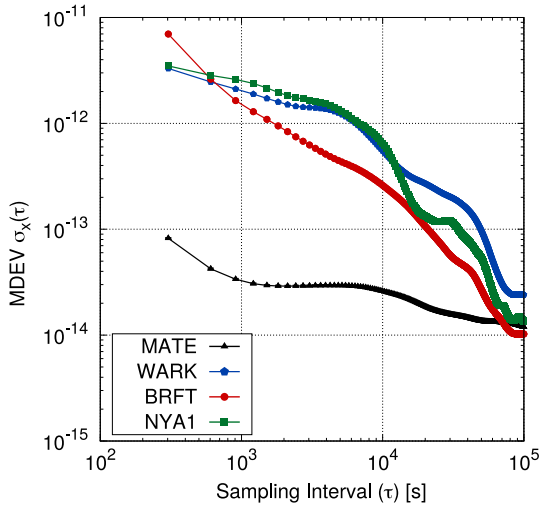

Figure 3.3: *Modified Allan Deviation (MDEV) for four different GNSS receiver clocks during the CONT17 campaign. BRFT stands for Fortaleza, WARK for Warkworth, MATE for Matera, and NYA1 for Ny-Ålesund.*

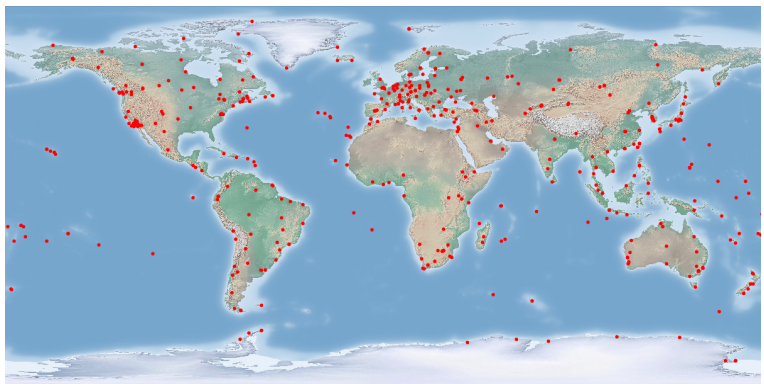

Figure 3.4: *The network of GNSS stations contributing to the International GNSS Service (IGS) (Kouba, 2009).*

The slant range observable, ρ, as shown in Eq. 3.5 is the norm of the vector difference and thus insensitive to the choice of reference frame. If a celestial reference frame were to be used, then a transformation of Earth-fixed satellite and receiver positions to that frame would need to take place, revealing the dependence of the observed slant range on EOP. The differential nature of this observable also shows that the precision of geodetic positioning of the ground-based segment is dependent and bounded by the precision of the space-based segment. The latter is in turn influenced by the presence of systematic errors which need to be estimated and removed. Common such errors are, e.g., the deficiencies in the models for gravitational and non-gravitational forces acting on the satellite orbits, or the presence of phase-center offsets of the satellite antennas that can be calculated after establishing a satellite-fixed nadir pointed reference frame.

It can be shown that (Rothacher et al., 1999)

$$\begin{aligned} \Delta(UT1 - UTC) &= -(\Delta\Omega + cos(i)\Delta u_0)/k, \\ \delta(\Delta\epsilon) &= cos(\Omega)\Delta i + sin(i)sin(\Omega)\Delta u_0, \\ \delta(\Delta\psi)sin(\epsilon_0) &= -sin(\Omega)\Delta i + sin(i)cos(\Omega)\Delta u_0, \end{aligned} \tag{3.6}$$

where ϵ_0 is the mean obliquity with respect to the ecliptic plane, $\delta(\Delta\epsilon), \delta(\Delta\psi)$ are the celestial pole offsets in obliquity and in longitude respectively, and k is the ratio between universal and sidereal times. The orbital parameters Ω, i and u_0 are defined in Sec. 2.1. When one refers to GNSS as unable to give access to certain EOP directly, namely $UT1$ and celestial pole offsets, it means that they cannot be separated from the systematic errors of the orbits themselves. This collinearity is manifested in Eq. 3.6, where the orbital elements and the aforementioned EOP are almost linearly dependent. The common way to mitigate this issue, is to estimate the time-derivative of those EOP that exhibit this behavior, or to tightly constraint the chosen datum of the respective EOP in the estimation process.

The small size and the simple design of GNSS antennas and receiver systems have facilitated the establishment of numerous permanent GNSS stations in a densified global network. The network of GNSS stations contributing routinely to the International GNSS Service (IGS) is shown in Fig. 3.4. The global distribution and ubiquity of these stations has a positive impact on the quality of space-geodetic products as it increases sensitivity to determining parameters of interest. An example of this is shown in Fig. 3.5, where the analysis of PM from the Center for Orbit Determination in Europe (CODE) is carried out (Dach et al., 2013). The contributions of IGS, therefore, have become vital with respect to the maintenance of ITRF, PM and LOD products (Altamimi and Collilieux, 2009).

3.3.1 The Era of multi-GNSS

The GNSS systems have come a long way since their inception in the 1950s. With the abolishment of selective availability (Zumberge and Gendt, 2001), higher accuracy satellite clock products were accessed with positive implications in research. The IGS continued its efforts to facilitate the access and processing of

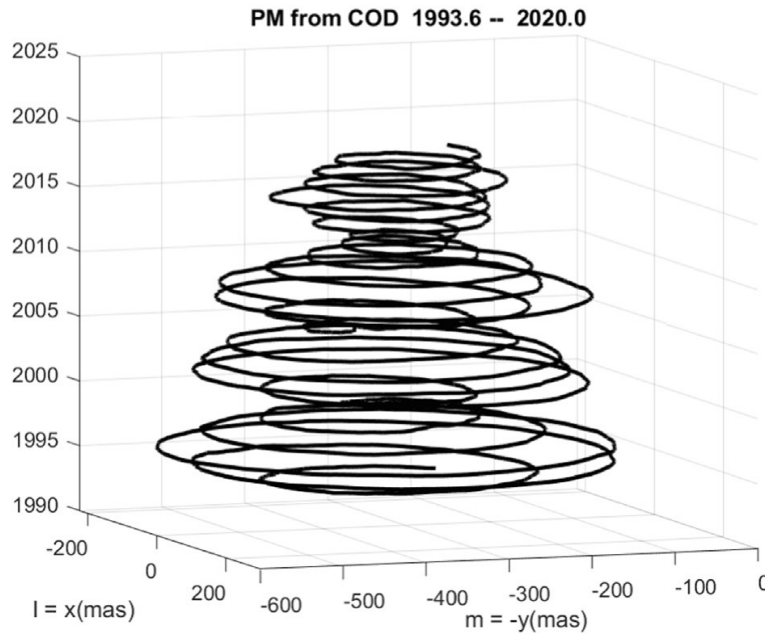

Figure 3.5: *GNSS-derived results covering for polar motion from 1993 to 2020 (Beutler et al., 2020).*

new signals and GNSS constellations as they became operational by establishing the Multi-GNSS Experiment (MGEX) (Montenbruck et al., 2017). Further developments include the update of the common observational data format, the Receiver Independent Exchange (RINEX) format, to newer versions that include multi-GNSS signals (Gurtner and Estey, 2007), and in parallel the distribution of precise products for multi-GNSS clocks and orbits via, e.g., CODE (Prange et al., 2016). The simultaneous and combined processing of signals from multiple GNSS constellations has shown to benefit the accuracy and precision of the acquired products, e.g., in the case of PPP both for ambiguity resolution and station position estimation (Aggrey and Bisnath, 2019; Xia et al., 2019).

Chapter 4

Very Long Baseline Interferometry

Radio interferometry developed as a concept in the early 60's in the attempt to characterize and study distant active galactic nuclei called quasars (Sovers et al., 1998). The precision required for such a task cannot be attained by single radio telescopes as their angular resolution, at a given frequency, is inversely proportional to, and constrained by the antenna diameter. For this reason, a technique was developed so that multiple separated antenna elements can be used increasing the effective diameter and gaining access to higher resolutions. The process behind it is based on constructive and destructive interference between waves of the same frequency. Two antennas that are physically separated but observe the same source, record coherent signals albeit with a time-delay. Through the process of correlation and as a result of constructive interference, this time-delay can be extracted. Since different sources are located in different points in the sky, the time-delay is unique for each of them and thus gives information about their position with respect to the baseline that the two antennas form. When this expands into a network of stations, the correlation between time-delays and baselines can be mitigated allowing for the determination of the source positions.

The concept was first demonstrated over relatively small distances (on the order of 1 km) in the form of the a connected element interferometer, where antennas can be connected to the same clock and the correlation can be performed in real-time (Preston et al., 1983). The evolution and increased stability of frequency standards, with the advent of the atomic clock, and of recording equipment, diminished the need for this partial connection between different elements of the interferometer. Instead, interferometers were constructed in a complete separate manner over long (on the order of hundreds to the low end of thousands of km) and very long distances (Whitney et al., 1976) resulting in so-called Very Long Baseline Interferometry (VLBI). The determination of precise source positions is vital for their subsequent study and lies within the field of astrometric VLBI, while the (inverse) procedure of observing a well-defined catalogue of source positions in order to define station positions is a goal of geodetic VLBI. The International VLBI Service (IVS) is the governing body for the upkeep and dissemination of high quality space-geodetic products derived from VLBI observations (Nothnagel et al., 2017).

4.1 Basic VLBI Observables

A simple two-element interferometer is presented in Fig. 4.1. A distant point-like source is emitting electromagnetic waves that arrive in a planar front at the receiving stations. The received signals, undergo amplification, downconversion and formatting before being recorded and sent to the correlation centres. The objective is to attain the main observable, the time-delay τ_d, which is predominantly attributed to the geometry between the receiving stations and the source. It can, therefore, be approximated by

$$\tau_d = -\frac{1}{c}\vec{s}\cdot\vec{b}, \tag{4.1}$$

where $\vec{s}$ and $\vec{b}$, are the source and baseline vector, respectively, expressed in the GCRS. Using Eq. 2.1, the baseline vector can be transformed to the ITRS equivalent meaning that the VLBI observables can be used to infer EOP. The signals in GNSS are transmitted at specified frequencies, show good signal-to-noise ratio (SNR) and their form, unmodulated by error sources like atmospheric refraction, is completely known to the receiver. The signals received by VLBI are weak and can be approximated best as band-limited white noise. This makes the process of determining the group and phase delays more challenging.

4.1.1 Correlation

The process of correlation can be described as follows. The signals, $u_1(t)$ and $u_2(t)$, (treated as continuous-time functions) are time-shifted with respect to each other, multiplied and averaged, i.e.,

$$\mathcal{R}(\tau) = \int_T u_1(t)u_2(t-\tau)dt, \tag{4.2}$$

where T is the integration time. Any choice of τ that causes the two signals to still be misaligned, leads to the multiplication generating another random signal and the subsequent integration averages it out. There exists, therefore a τ, which maximizes the value of $\mathcal{R}$ and corresponds to the observed time-delay. Using Fourier transformation of Eq. 4.2, the (angular) frequency-dependent cross-power spectrum of the two signals can be obtained as

$$S_{u_1u_2}(\omega) = A(\omega)e^{i\Phi(\omega,t)}, \tag{4.3}$$

where for a reference angular frequency ω_0 and reference time t_0

$$\Phi(\omega,t) = \Phi_0(\omega_0,t_0) + \frac{\partial\Phi}{\partial\omega}(\omega-\omega_0) + \frac{\partial\Phi}{\partial t}(t-t_0), \tag{4.4}$$

with $\tau_g = \frac{\partial\Phi}{\partial\omega}$ the group delay, and $\Phi_0(\omega_0,t_0)$ a phase ambiguity term. The different effects that dominate the correlation process can be seen in Eq. 4.4, namely the delay-rate term which corresponds to the diurnal motion of the source with respect

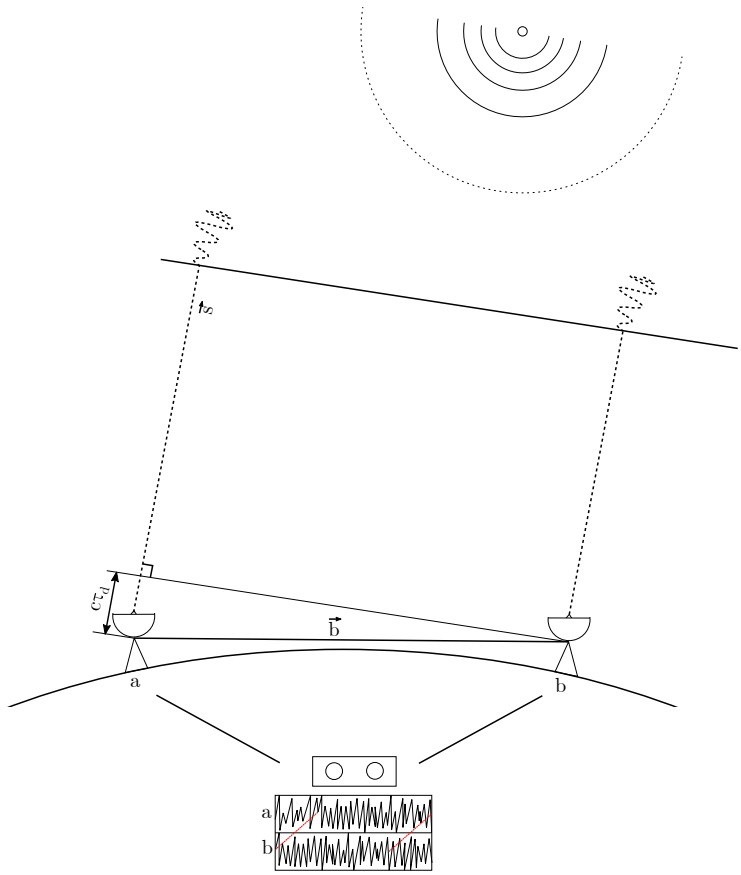

Figure 4.1: *The geodetic concept of VLBI observations. A planar wave front emitted from a distant radio source is received at two stations forming a baseline. The signals are recorded and subsequently correlated to extract the time-delay by matching the common patterns.*

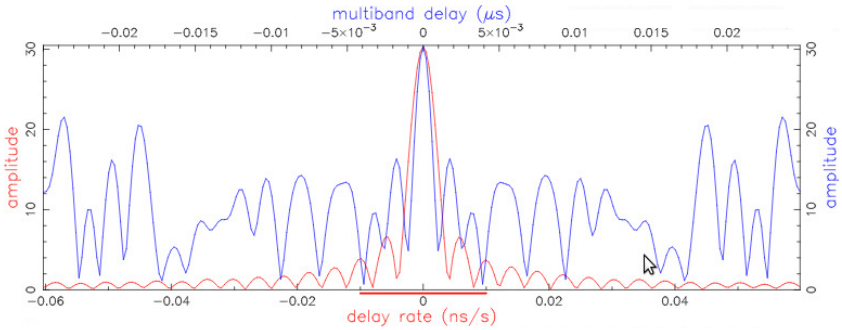

Figure 4.2: *The residual multi-band delay and delay-rate for an X-band observation between the 20 m legacy telescope and one of the new generation VLBI Global Observing System (VGOS) telescopes, at Onsala (Sweden). The fringe-fitting has been carried out with the fourfit software (Cappallo, 2017).*

to the baseline, and the frequency-dependent term which if too high will cause the so-called fringe pattern at the correlator output to oscillate rapidly impeding the correlation process. It is thus desirable to use an a priori guess of the group delay, τ_i, calculated through the delay model, and subtract it from the group delay $\delta\tau_g = \tau_g - \tau_i$, as well as an estimate of the delay-rate term in the same manner, to reduce Eq. 4.4 to the residual fringe phase defined as

$$\Delta\Phi(\omega, t) = \Phi_0(\omega_0, t_0) + \delta\tau_g(\omega - \omega_0) + \Delta\frac{\partial\Phi}{\partial t}(t - t_0), \tag{4.5}$$

with the residual group delay $\delta\tau_g$ and the the residual delay rate, $\Delta\frac{\partial\Phi}{\partial t}$. This is an effective way of reducing the search window during correlation. Substituting the residual fringe phase into Eq. 4.5 and performing an inverse Fourier transformation reveals the fringe pattern. In particular, the latter takes the form of $A\cos\Delta\Phi$ where $\Delta\Phi$ is principally driven by the residual group delay and delay rate. Thus, correct resolution and compensation lead to it maximizing and producing a fringe pattern, as shown in Fig. 4.2. Since the VLBI signal is weak, travelling through the signal chain can distort it enough so that the correlation process is unsuccessful. For this reason, the fringe fitting process has to account for instrumental delays as well. The principal way of tackling this issue is to inject a signal of known phase before the LNA and measure the phase shift (phase-cal).

After the residual fringe phase, group delay and delay-rate have been established, they are added to the instrumental delays used in order to get the total values and hence the three observables, namely the delay-rate $\frac{\partial\Phi}{\partial t}$, the group delay $\frac{\partial\Phi}{\partial\omega}$ and the fringe phase $\Phi(\omega, t)$. Note that the latter contains the cycle ambiguity which prevents from it being used in a straightforward manner. The determination of the time-delay per frequency channel gives what is known as single-band delay (SBD). After the SBDs have been obtained, a process of determining a common delay over all channels is carried-out, giving the multi-band delay (MBD). This is accomplished through the bandwidth synthesis technique (Kondo and Takefuji,

2016; Shaffer, 2000). The uncertainty of the multi-band group delays is given as (Shaffer, 2000)

$$\sigma_{\tau_g} = \frac{1}{2\pi SNR f_{rms}}, \tag{4.6}$$

where f_{rms} is equal to the root mean square of the frequency span or 40 % of the total bandwidth.

Summarizing, the correlation process can be described as follows. The signal, collected in two stations forming a baseline, can be approximated as band-limited white noise. Such a characterisation means that one can think of it as a set S of monochromatic signals of different frequencies. A subset $S_s \subset S$ of them is what the source is emitting while the rest are noise. Through the process of correlation the signal of one station is shifted with respect to the reference station of the baseline, until the subsets S_s of the two signals align in time. This is accomplished when the cross-correlation of the signals maximizes, i.e., their multiplication and averaging removes the noise and amplifies the common patterns.

4.1.2 Scheduling

It is evident, looking at the characteristics of the correlation procedure, that a high SNR can be achieved for (a) long integration times which have a positive effect on averaging out noise, (b) large bandwidth which means more monochromatic components of the source signal. The value of SNR can be further augmented by the observation of point-like bright sources, low system noise and a large amount of channels. This is indeed true as (Shaffer, 2000),

$$SNR = \frac{\eta_c S_f}{\sqrt{SEFD_1 SEFD_2}} \sqrt{2 B_{ch} N_{ch} T}, \tag{4.7}$$

where $SEFD$ is the system equivalent flux density and is related to system noise temperature of the receiving system normalised by the effective area of the antenna. S_f is the flux density of the radio source, η_c an efficiency factor for sampling and correlation, while N_{ch} and B_{ch} are the number of channels and channel bandwidth respectively. The need arises, when talking about an interferometric network of stations, for scheduling that optimizes for the aforementioned parameters. Since the networks need to have a worldwide distribution, it might mean that subnets of stations are formed during the observation process. For geodetic VLBI experiments, schedules are produced by specialised software, namely *Sked* (Gipson, 2010) and *VieSched++* (Schartner and Böhm, 2019) which output so-called *.skd* files. The files contain not only the observation schedule but also the sampling mode, and the frequency channel setup, i.e., bandwidth number of channels and center frequency per band.

4.2 VLBI Delay Model

The delay as expressed in the simplified form of Eq. 4.1 is augmented with the influence of certain physical phenomena. The change of the ray path due to the

gravitational attraction that it experiences as it passes by of our solar system must be accounted for. The general relativistic term added to the simple delay model is

$$\Delta T_{grav} = \sum_j \Delta T_{grav_j}, \tag{4.8}$$

where j refers to a specific gravitational body (Petit and Luzum, 2010)

$$\Delta T_{grav_j} = 2\frac{GM_j}{c^3} ln \frac{|\vec{R_{1j}}| + K\vec{R_{1j}}}{|\vec{R_{2j}}| + K\vec{R_{2j}}}, \tag{4.9}$$

with $\vec{K}$ the unit vector from the barycenter to the source and R_{ij} the vector from j^{th} gravitational body to the i^{th} receiver. The latter are given for a single baseline as (Petit and Luzum, 2010)

$$\begin{aligned} R_{1j} &= \vec{X_1}(t_1) - \vec{X_j}(t_{1j}), \\ R_{2j} &= \vec{X_2}(t_1) - \frac{V_\oplus}{c}\vec{K}\cdot\vec{b} - \vec{X_1}(t_{1j}). \end{aligned} \tag{4.10}$$

It follows that in the case of Earth, these vectors correspond to the geocentric vectors, i.e., the coordinates expressed in the GCRS. The barycentric coordinates of a receiver i can be retrieved by a simple translation of the origin from the geocenter to the barycenter (Petit and Luzum, 2010)

$$\vec{X_i} = \vec{x_i}(t_1) + \vec{X}_\oplus(t_1), \tag{4.11}$$

while t_{1j} is equal to

$$t_{1j} = \min\Big[t_1 - t_1\frac{\vec{K}\cdot(\vec{X_j}(t_1) - \vec{X_1}(t_1))}{c}\Big]. \tag{4.12}$$

The geocentric delay due to geometry, in vacuum, can be expressed as (Petit and Luzum, 2010)

$$t_{v2} - t_{v1} = \frac{\Delta T_{grav} - \frac{\vec{K}\cdot\vec{b}}{c}[1 - \frac{(1+\gamma)U}{c^2} - \frac{|\vec{V}_\oplus^2|}{2c^2} - \frac{\vec{V}_\oplus\cdot\vec{w}_2}{c^2}] - \frac{\vec{V}_\oplus\cdot\vec{b}}{c^2}(1 + \vec{K}\cdot\vec{V}_\oplus/2c)}{1 + \frac{\vec{K}\cdot(\vec{V}_\oplus + \vec{w}_2)}{c}}, \tag{4.13}$$

where U is the gravitational potential at the geocenter, neglecting Earth's mass. The delay term should include the geometric atmospheric effect visible in Fig. 2.2b and corresponding to the G term in Eq. 2.4 and given as (Petit and Luzum, 2010)

$$t_{g2} - t_{g1} = t_{v2} - t_{v1} + \delta t_{atm_1}\frac{\vec{K}\cdot(\vec{w}_2 - \vec{w}_1)}{c}. \tag{4.14}$$

In conclusion the delay model is

$$\tau_d = t_{g2} - t_{g1} - t_{clk} - t_T - t_I - t_{misc}, \tag{4.15}$$

containing further the clock offsets, t_{clk}, the non-geometric term of the atmospheric refraction, t_T referring to the troposphere and t_I to the ionosphere. Miscellaneous error sources like the misalignment of the lateral displacement of the two principal axes of rotation of a telescope in a X/Y mount or the thermal and gravitational deformation of the antennas which result in additional delays (Nothnagel et al., 2019; Nothnagel, 2009; Wresnik et al., 2007) represented by t_{misc}. This term also includes errors induced by the frequency-dependent positional variation of radio sources, an outcome of their non-perfectly point-like nature (Anderson and Xu, 2018). Better modelling of effects that contribute to t_{misc}, like that of galactic aberration (MacMillan et al., 2019), help resolve them and produce a more robust delay model.

4.3 Data Analysis

The troposphere and the ionosphere can be modelled and estimated as discussed in Sec. 2.3. For the legacy VLBI systems the existence of two bands (S/X) makes it possible to obtain the ionospheric-free linear combination reflecting the similar process that happens in GNSS as shown in Eq. 2.6. The differential nature of the observables means that during data analysis a clock datum must be established and offsets with respect to this datum must be calculated. In addition, for the determination of station positions of a VLBI network, in a routine least-squares (LSQ) fit, an observation equation

$$A \cdot x = y, \tag{4.16}$$

where A is an $n \times m$ matrix linking, n observations to m estimable parameters. A set of normal equations (NEQ) is constructed of the form

$$N \cdot x = b, \tag{4.17}$$

where $N = A^T P A$ is an $m \times m$ so-called normal matrix and $b = A^T P y$, and P the variance-covariance matrix.

4.3.1 Datum Constraints

The matter of fact is that when solving for station positions and EOP there exists a rank deficiency in the normal matrix of Eq. 4.17. This means that not all parameters are linearly independent with respect to each other, which is motivated by the differential nature of interferometric measurements. In other words, VLBI analysis realises a frame which, unless some form of constraining is applied, lacks information on the position of its origin, when solving for station positions only, and also of how it is oriented when additionally estimating EOP. The solution should be that the estimated realisation of the frame must be constrained to an a priori one. This can be done by either fixing stations to their a priori positions, constraining the estimated correction to the a priori coordinates, a free-net solution, or by applying the minimal set of constraints needed so that the rank deficiency is

accounted for. The latter approach is called Minimal Constraints (MC). The MC approach seeks to nullify the Helmert transformation parameters between the two realisations of the frame. In particular, the estimated coordinates $(\tilde{x}_1, \tilde{y}_1, \tilde{z}_1, ..., \tilde{z}_n)$ are related to the a priori coordinates, $(x_1, y_1, z_1, ..., z_n)$, through the following similarity transformation (Sillard and Boucher, 2001)

$$\begin{pmatrix} \tilde{x}_1 \\ \tilde{y}_1 \\ \tilde{z}_1 \\ \vdots \\ \tilde{z}_n \end{pmatrix} = \begin{pmatrix} x_1 \\ y_1 \\ z_1 \\ \vdots \\ z_n \end{pmatrix} + \begin{bmatrix} 1 & 0 & 0 & x_1 & 0 & -z_1 & -y_1 \\ 0 & 1 & 0 & y_1 & z_1 & 0 & x_1 \\ 0 & 0 & 1 & z_1 & y_1 & -x_1 & 0 \\ \vdots & & & & & & \\ 0 & 0 & 1 & z_n & y_n & -x_n & 0 \end{bmatrix} \cdot \begin{pmatrix} T_x \\ T_y \\ T_z \\ s \\ R_x \\ R_y \\ R_z \end{pmatrix}. \tag{4.18}$$

Since it is a linear relation with respect to the three translation parameters T_x, T_y, T_z, the three rotation parameters R_x, R_y, R_z, and the scale parameter s, as evident in Eq. 4.18, the partial derivatives can be acquired in a straightforward way. They can be then appended on the otherwise singular matrix N so that the augmented matrix does not have rank deficiency (Altamimi et al., 2002). The resulting constraints are called no-net-translation (NNT) for nullifying the translation parameters, no-net-rotation (NNR) for nullifying the rotation parameters and no-net-scale (NNS) for nullifying the scale parameter. The advantage of this technique with respect to the others is that it retains information on the estimable characteristics of the geodetic network without deforming the geometry as defined by the observations. Different methods can be applied to mitigate a poor choice of an a priori frame, referred to as datum noise, or poor quality of observations, i.e., data noise (Kotsakis, 2018).

4.3.2 Parameter Constraints

Augmenting the normal matrix N of Eq. 4.17 with additional constraints is not limited to defining a geodetic datum. Data gaps that may appear due to downtime in one or multiple VLBI stations, increased radio frequency interference (RFI) in one or several observing channels, discontinuities in the clock parameters introduced at the correlation stage to facilitate fringe pattern extraction, lead to singularities in the LSQ formulation. Constraining the unresolvable parameters of interest, helps mitigate these issues and is usually done either on themselves or their rates. The constraints are input as pseudo-observations and the normal matrix is augmented to accommodate for the new dimensionality (Artz et al., 2016).

4.4 VLBI in Space Geodesy

VLBI is the only technique in Space Geodesy that observes extragalactic sources and as such, it can have access to all EOP. This has made it an invaluable contributor to high quality space-geodetic products. Observations usually span 24 hours, and the quality of their products dependent on the polyhedron the observing network

is covering (Malkin, 2009). Examples of geodetic VLBI sessions that are organised regularly by IVS are:

- The *IVS-R1* and *IVS-R4* sessions that take place two times per week and are comprising of a modest set of 7-9 stations and are designed to be used for EOP estimation.
- The intensive (*INT*) sessions on baselines, Wettzell (Germany) to Kokee Park (USA), called *INT1*, and Wettzell (Germany) to Ishioka (Japan) called *INT2*, which aim at $UT1 - UTC$ and last 1 hour. There is also and intensive series network comprising of Wettzell (Germany), Ishioka (Japan) and Ny-Ålesund (Norway). Due to the unpredictable nature of $UT1 - UTC$, the measurements are taken daily.
- The *IVS-T2* sessions aiming at TRF which comprise of a more populous network of 14-18 stations and take place at least twice a year.
- The *R&D* sessions which take place every month and aim to investigate and study instrumental effects and product improvement.
- The two week continuous VLBI observations, *CONT* sessions, involving a comprehensive network with the largest volume of polyhedron formed. These measurements have recently been discontinued, in the transition to the next-generation radio telescopes for geodetic VLBI.

4.4.1 The Era of VGOS

The long-standing equipment for VLBI observations, the so-called S/X systems, had been developed in the 1970s. Over the years, the advancements in electro-mechanical systems that allow for the construction of faster-slewing radio telescopes, the development of wideband receivers that give the opportunity to observe over a wider range of frequencies, along with challenges like increased radio frequency interference in the lower observing bands, have motivated the need for the realization of a state-of-the-art VLBI station. This need was recognized with the VLBI2010 initiative (Petrachenko et al., 2009), that described the concept of the next-generation VLBI systems, and is being realized with the construction of the VLBI Global Observing System (VGOS) network of stations (Behrend et al., 2019). The main design goals were (a) a broadband (2-14 GHz) dual-polarization observing capability which in turn allows for shorter integration times, and (b) faster slewing rates (up to 12 ^{o}/s) which can take advantage of the short scan times to provide an increased observation cadence and more diverse sky mapping. The VGOS operations are the IVS contribution to the realization of the multi-technique Global Geodetic Observing System (GGOS) concept (Rothacher et al., 2009). The currently deployed VGOS network can be seen in Fig. 4.3. The IVS session setup for VGOS comprises of:

- The *VO* sessions which are the 24 h VGOS operational sessions.

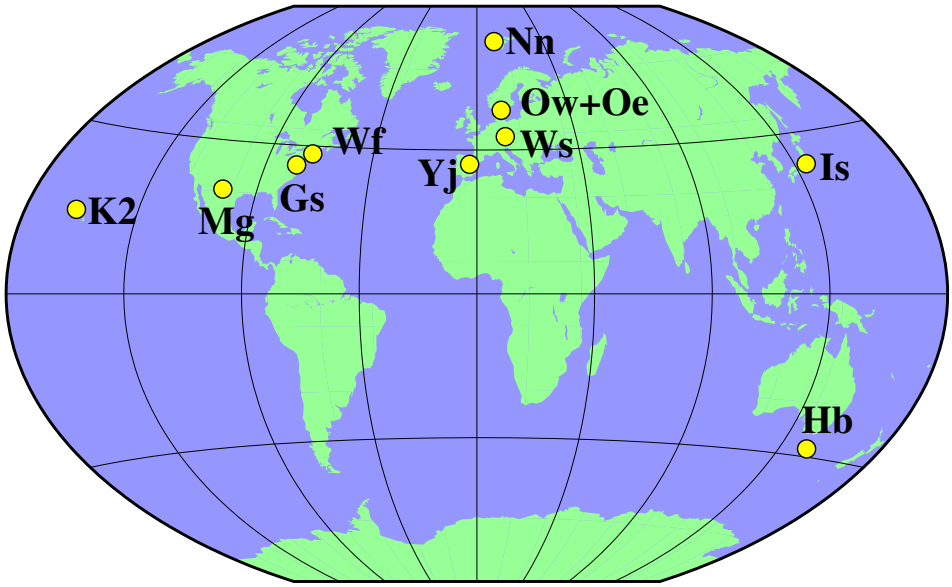

Figure 4.3: *The operational VGOS network as of early 2023.*

- The *VGOS-B* and *VGOS-2* sessions which are 1 h intensive sessions.
- The *VR* sessions which are the VGOS Research and Development sessions.

Chapter 5

Combination of Space-geodetic Techniques

Space-geodetic techniques, apart from positioning determination, can be used for the definition of reference frames through the determination of their origin, orientation and scale. A single technique, however, cannot uniquely define a frame. In the case of the ITRF (Altamimi et al., 2016), the origin of the frame, i.e., the geocenter is primarily accessed through SLR. The scale parameter is determined from both VLBI and SLR, and the orientation is defined through an MC approach incorporating observations from all four techniques with respect to previous realisations of the ITRS. It is evident, therefore, that for a proper frame definition, a combination of multiple space-geodetic techniques is essential.

Even when the primary goal is not the realisation of a reference system, the simultaneous processing of multiple techniques facilitates the transfer and the increase of frame information among them, like, e.g., access to SLR-derived geocenter by GNSS (Thaller et al., 2011). The concept of co-location sites, i.e., sites which contain several space-geodetic instruments (stations) becomes crucial in this context since, these stations share frequency standards in the form of common clocks and feature similarity in atmospheric refraction phenomena. Combination featuring these sites leads to an improvement in, e.g., inter-continental frequency transfer (Hobiger et al., 2015) and in overall quality of parameters of interest like station positioning or EOP through the better resolution of tropospheric delays (Krügel et al., 2007). Combined networks allow for the densification and better geometry of the attained observation set and ensure overall robustness since common parameters are simultaneously inferred from independent techniques. The latter, especially, helps with mitigating technique-specific biases, like e.g., mismodelling of phase center correction for GNSS antennas and the effect it has on tropospheric delay determination (Ejigu et al., 2019). Ultimately, by the application of common displacement models and simultaneous determination of common parameters of interest, combination allows for consistency and homogeneity in the problem formulation which benefits the precision and quality of space-geodetic products.

5.1 Combination Strategies

Three main strategies are used when attempting a combination of multiple space-geodetic techniques, namely (a) combination on the results level, (b) combination on the normal equation level and (c) combination on the observation level.

5.1.1 Combination on the Results Level

Combination on the Results Level (CRL) is routinely employed for the successive iterations of the ITRF(Altamimi et al., 2011, 2016; Boucher et al., 2004). In the context of frame definition it works as follows. Single-technique solutions which span several years of data are carried out at first and time series of station positions, velocities and EOP are generated. The produced results are then input into a combined problem which contains a 14-parameter similarity transformation, similar to the Helmert transformation presented in Eq. 4.18 in Sec. 4.3.1, but expanded to the rates of the translation, rotation and scale parameters. In the formulated problem at this second stage, all single-technique acquired parameters are used as observations with a combined solution analog being produced as a result. In this strategy, as station positions and EOP are first computed independently, there is no possibility of capitalising on commonalities in co-location sites, like frequency standards or atmosphere. The convergence points between the different techniques are instead (a) the common frame-defining parameters, (b) the common EOP and (c) the existence and utilisation of so-called local ties (LT), elaborated in Sec 5.2, at co-location sites. The single-technique time-series undergo a pre-combination process where they are evaluated in the context of the velocity fields they produce between adjacent stations, enabling for their homogenisation and outlier removal. The latest iterations of this technique also include post-seismic as well as displacement models and modelling and mitigation of seasonal variations on the station position signal caused by geophysical loading phenomena or system-specific biases like, e.g., draconitic periods of satellite orbits in GNSS (Altamimi et al., 2016; Griffiths and J. R. Ray, 2013).

5.1.2 Combination on the Normal Equation Level

The single-technique analysis step before the main combination which is present in CRL, gives the ability to the analyst to evaluate these interim results and to remove discontinuities or irregularities. On the other hand, this process does not take into account some important information that stems from the common error sources at co-location sites. The correlation between these error sources and parameters of interest is invariably lost along with what better resolution of them demonstrably offers (Hobiger and Otsubo, 2015). Combination on the Normal Equation Level (CNL) has been developed to mitigate this issue. In this approach, the following steps are performed, namely (a) a set of datum-free NEQ is constructed for each technique which are then, (b) modified by pre-eliminating parameters that correspond to error sources, (c) put together through the process of so-called stacking, and (d) append datum information using an approach like

MC (Thaller, 2008). Starting from the Eq. 4.17, the process of pre-elimination is splitting the normal matrix N between parameters of interest x_1 and nuisance parameters x_2 as

$$\begin{bmatrix} N_{11} & N_{12} \\ N_{21} & N_{22} \end{bmatrix} \begin{pmatrix} x_1 \\ x_2 \end{pmatrix} = \begin{pmatrix} b_1 \\ b_2 \end{pmatrix}, \tag{5.1}$$

which is essentially a system of two linear equations,

$$\begin{aligned} N_{11} \cdot x_1 + N_{12} \cdot x_2 &= b_1, \\ N_{21} \cdot x_1 + N_{22} \cdot x_2 &= b_2, \end{aligned} \tag{5.2}$$

where x_2 can be eliminated by a linear combination of the system resulting in the reduced expression

$$(N_{11} - N_{12}N_{22}^{-1}N_{21}) \cdot x_1 = b_1 - N_{12}N_{22}^{-1} \cdot b_2. \tag{5.3}$$

So CNL, in contrast to CRL, through the construction of a unified set of normal equations, retains the essential information and correlations between the target parameters and those which pertain to error sources allowing for the combination approach to fully exploit this trait for stations that are co-located.

5.1.3 Combination on the Observation Level

The Combination on the Observation Level (COL) is close in definition to CNL as it can be approached by means of constructing and stacking NEQ. The main differences lie firstly in the fact that COL lacks a pre-elimination process which means that all technique-specific parameters are reachable by the analyst (Biancale et al., 2010). And secondly, in the consistency and homogeneity of the a priori information and models used and the historical development of data analysis using these techniques. In the absence of multi-technique space-geodetic softwares like, e.g., $c5++$ (Hobiger et al., 2010), the analysis centres construct a technique-specific set of datum-free NEQ as a first step in a two-step process. Then, these equations are sent to the combination centres, where CNL is performed. The ability to analyze several space-geodetic observables within one software package means that the generation and process of combined NEQ can be done in one step, ensuring the highest level of consistency between them (Artz et al., 2012; Thaller, 2008). In this context, in Paper I, a COL was attempted using VLBI and GNSS in inter- and intra-technique modes to evaluate TRF and EOP products. The GNSS and VLBI were linked without local ties but via common atmosphere, while two VLBI networks are linked with common EOP. More details follow in Sec. 6 (Diamantidis et al., 2021).

5.1.4 Combination Software

The $c5++$ multi-technique space-geodetic software (Hobiger et al., 2010) has been used for the studies conducted in the appended papers. It was augmented with a kalman filtering module for both multi-GNSS and VLBI estimation. This

implementation was tested for the individual techniques as shown in papers III and V of this thesis. Paper III deals with 3 years of VGOS-O sessions, evaluating EOP and station position estimates, while Paper V studies tropospheric gradient products obtained from multiple co-located GNSS antennas, and compares them to the ones obtained from a co-located Water Vapor Radiometer. More details are given in Sec. 6

5.2 Troposphere Ties

The existence of co-location sites is of uttermost importance both in the CRL and the CNL techniques. The CRL method is capitalizing on the fact that it is in these sites where LT between the different co-located space-geodetic stations are measured. These are then input in the combination problem to merge the single-technique solutions and attain a common frame definition. The CNL method is attempting to additionally utilize the heterogeneous space-geodetic observables in order to estimate common error sources. One such error source, in microwave-based techniques, is the elongated signal path due to atmospheric refraction as discussed in Sec. 1.3.1, and expressed through the estimation of the Zenith Wet Delay (ZWD) and tropospheric gradient (GRN/GRE) parameters. The introduction of tropospheric ties between VLBI and GNSS, i.e., determining common ZWD and GRN/GRE, has shown to greatly benefit the precision and accuracy of the derived geodetic products (Diamantidis et al., 2021; Hobiger and Otsubo, 2015; Thaller, 2008; J. Wang et al., 2022b). The increased observational cadence and augmented geometry that the combined datasets provide, results in a more accurate determination of the tropospheric delay, which has a knock-on effect on the accuracy of all estimated parameters that are correlated to it. The ZWD parameter, for example, is particularly correlated to station position estimates and especially the local vertical component, while tropospheric gradients resolve the station position in the local horizontal plane (J. Wang et al., 2022b). The tropospheric gradients are also correlated to EOP. Their impact on UT1-UTC determination in the context of the 1 h VLBI intensive sessions has been extensively studied (Böhm et al., 2010; Landskron and Böhm, 2019; Teke et al., 2015), and the possible gains of troposphere ties with GPS has been illustrated (J. Wang et al., 2022a). The Paper II contribution takes this concept one step further by introducing multi-GNSS into the combination (Diamantidis et al., 2022). In particular we utilized the augmented geometry that multiple GNSS constellations offer, and created a 3 h “shell” of GNSS data that envelops symmetrically time-wise the VLBI intensive session. We then studied the impact that the enhanced tropospheric gradient estimation had in the precision and accuracy of the UT1-UTC determination both for legacy S/X and VGOS intensives. The effects of incrementally adding GNSS constellations in the estimation were explored as well. More details are presented in Sec. 6.

5.3 Local Ties

The combination strategies essentially seek to find and exploit commonalities between the different space-geodetic techniques. In CRL, in particular, where single-technique solutions provide a set of station positions, velocities and EOP, it is evident that each technique generates its own frame definition. The objective of combination in this sense is to find an "optimum" average of these. While the same applies for EOP, this is not the case for station positions since they are inherently different. Additional observations that attempt to establish a link between station positions can, therefore, strengthen the combination procedure. This is what LT, i.e., a set of three dimensional measurements between stations at co-location sites, contribute. Despite the fact that LT are very precise and can reach millimeter level accuracy, discrepancies on the centimeter level can be detected between them and the ITRF-derived distances (Altamimi et al., 2016; J. Ray and Altamimi, 2005). Technique-specific error sources contribute also to discrepancies between LT and distances obtained through single-technique solutions (Nothnagel et al., 2019).
The LT information is input as a pseudo-observation

$$\begin{pmatrix} x \\ y \\ z \end{pmatrix}_{tie} = \begin{pmatrix} x \\ y \\ z \end{pmatrix}_{i} - \begin{pmatrix} x \\ y \\ z \end{pmatrix}_{j}, \tag{5.4}$$

where i and j represent different stations at the same co-location site.

Proper evaluation and weighting of the LT is thus essential in order for them to contribute to the combination in an effective manner. The weighting is commonly done in an iterative empirical manner by either inspecting post-fit residuals (Altamimi et al., 2016) or by evaluating the effect of LT in the EOP estimation. Inspection of $UT1 - UTC$ estimates for a combination between VLBI and GNSS stations by incorporating different ties shows that beneficial tie information results in improved station position repeatabilities without affecting the mean correction of $UT1 - UTC$ estimates with respect to a priori values (Thaller, 2008).

5.3.1 A Novel Approach to Combination

As described in Sec. 5.3 LT are essential in providing an innate link between inherently different parameters like the positions of different stations at a co-location site. Ultimately, they need to be adjusted and weighted as they represent different optima from the positions derived through the means of Space Geodesy. While the latter are obtained from a global solution and represent the optimal values that provide the most stable frame definitions, tie measurements reflect the absolute precision at a local level. It is also evident by Eq. 5.4 that an attempt to estimate station positions utilizing only LT would result in a rank deficient problem.

These two realisations motivate a new strategy. The geometric link between stations at a co-location site becomes a primary parameter of interest instead of an aiding pseudo-observation in the combination process (Fig. 5.1). This means that

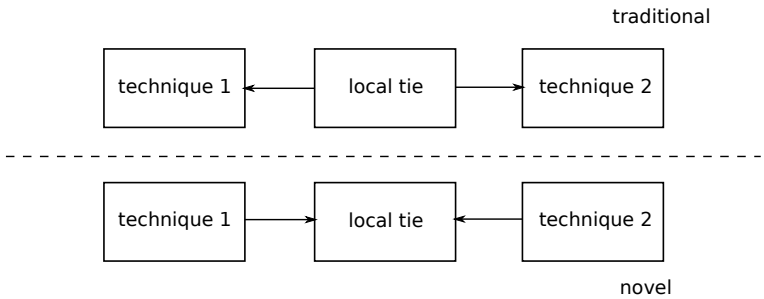

Figure 5.1: *Conceptual difference for the utilisation of local ties between traditional and novel techniques. The traditional technique estimates station positions of co-located stations augmenting the problem with local ties as independent measurements. The novel one estimates the common vector between co-located stations using local ties as measurements to directly observable parameters. Details are presented below.*

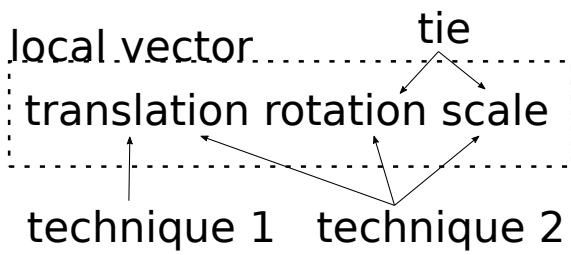

Figure 5.2: *The novel technique focuses on estimating the translation, rotation and scale of the local vector. While translation is linearly dependent to rotation/scale, this dependency is mitigated by a clear distinction of how the observations are used in the construction of the LSQ problem. The high-frequency first technique is driving the estimation of the translation parameter, while the local ties are used to clearly disassociate the rotation/scale parameters from it.*

a problem reformulation is carried out as follows. A station is chosen as the origin of the local vector, and it is the one that corresponds to the technique with the highest frequency of observations, i.e., GNSS, for reasons that will be explained further. What would normally be the correction to GNSS station positions, now corresponds to the translation of the local vector. The second co-located technique is used to sense both the translation of this vector as well as its rotation and scale. The motivation behind this is as follows. First, the rotation/scale of the local vector and translation of its origin are linearly dependent and artificially decoupling them is physically inconsistent, as in every iteration of the estimation procedure the point of the origin is the basis on which rotation/scale will be determined. Second, the co-located space-geodetic stations are subject to common high-frequency or non-tidal loading effects, and thus their respective station position variations could be correlated. This would mean that the second co-located technique can estimate both (a) the station position variations of the first, and (b) the relative displacement between the two. Such an endeavor introduces a collinearity which is mitigated twofold and can be seen in Fig. 5.2. The translation of the local vector is simultaneously provided and primarily driven by the high-frequency technique, in this case GNSS, akin to a "high-low" configuration in sensor fusion. The rotation and scale are independently accessed through the local tie measurements. In particular, the a priori positions are used to calculate the (a priori) local vector which is compared to the one obtained from the LT, extracting equivalent "local tie" rotation and scale parameters. They are, then, utilised as pseudo-observations with respect to the estimated rotation R_x, R_y and scale s of local vector between stations i and j,

$$\begin{pmatrix} s \\ R_x \\ R_y \end{pmatrix}_{tie} = \begin{pmatrix} s \\ R_x \\ R_y \end{pmatrix}_{ij} . \tag{5.5}$$

This constitutes a major departure in the utilisation of LT, since they are used to observe what they inherently are instead of the differential nature of two primary parameters of interest that Eq. 5.4 dictates.

Paper IV of this thesis is exploring this concept (Diamantidis et al., 2023). Firstly, the existence and the extend of correlation in station position variations between co-located stations were studied. This was followed by introducing the Combination Using a Single Point (CUSP) method and conducting a proof of concept study with it. The technique was tested during the continuous 15-day CONT17 VLBI campaign (Behrend et al., 2020) for a COL between the VLBI and co-located GNSS stations using the $c5++$ space-geodetic software. Common atmosphere was estimated and LT were used in the traditional and novel frameworks of formulating them. All but two ties were utilised and no empirical tuning was applied. A summary is presented in Sec. 6.

Chapter 6
Summary and outlook

This thesis has presented general topics that are pertinent in any space-geodetic analysis along with the specific working principles of two space-geodetic techniques, VLBI and GNSS, their contributions to space-geodetic products and their role in the realisation of the ITRF. The concept of combination was then explored, looking at the different techniques used and their limitations with respect to LT utilisation. A novel approach for multi-technique combination was presented along with a proof of concept. The work should expand on multiple fronts. Firstly, the multi-GNSS processing must be refined using (a) state-of-the-art methods for phase ambiguity resolution, (b) all available signal combinations and/or raw observations, (c) orbit estimation. Secondly, the VGOS observations should be further studied with respect to a VGOS-derived CRF product. Finally, the concept of co-location in space (Anderson et al., 2018) should be included by incorporating and studying the topic of Precise Orbit Determination (POD) (Klopotek et al., 2020).

Summary of Paper I

The topic of COL was examined in two different ways, using the continuous VLBI campaign CONT17 as a dataset. Firstly, a COL on the level of common atmosphere between the Legacy-1 VLBI network that participated in CONT17 and the co-located GNSS stations, where the precision of derived station position was compared with respect to single-technique solutions. Secondly, the two legacy VLBI networks of CONT17 were combined on the level common EOP, and the accuracy of the derived PM, between the two combination schemes with respect to IGS products, was evaluated.

Summary of Paper II

We performed COL with common troposphere in the context of the legacy S/X and VGOS intensive sessions. In particular, the VGOS-B sessions between December 2019 and February 2020 and the concurrently observed INT1 sessions were analyzed. We combined each session of these datasets with 3 h multi-GNSS data that uniformly

envelop them and combined them in the context of zenith wet delay and tropospheric gradients. We then evaluated the results in the folowing ways. We looked at the effect on the precision of the estimates and the relative agreement between concurrently observed sessions. We studied the effect of incrementally adding GNSS constellations in the combination, as well as estimating tropospheric gradients more frequently. We generated correlation plots between the estimated corrections to the a priori UT1-UTC and the tropospheric parameters. We finally compared the results to those that would be acquired if, instead of combining with multi-GNSS, the tropospheric parameters were estimated offline and given as a priori to the VLBI data analysis.

Summary of Paper III

The first three years of the VGOS-O 24 h sessions were analyzed using the kalman filtering approach, and as independent daily solutions. The ITRF2020, the c04-20 EOP series, and the ICRF3 were initially utilized as a priori TRF, EOP and CRF respectively. The ICRF3 has been determined using legacy S/X observations which differ in observing frequency bands with respect to VGOS observations, and the location of the radio source brightness centres is frequency-dependent. This means that VGOS observations are rich in radio source position information, which if unresolved, might introduce spurious effects in EOP determination. For this reason, and using the 3 year dataset, we generated a VGOS-adjusted ICRF3 (VA-ICRF3) by solving for radio source positions. We produced two flavors of this VA-ICRF3, one which was generated using a no-net-rotation constraint on a subset of the defining sources, and one with an additional soft constraint on celestial and terrestrial pole offsets. We then compared the frame defining parameters of these two with respect to ICRF3 and found the second one to be more stable. We proceeded to utilize this and reprocess the data, and evaluated the results in terms of mean biases of the obtained EOP. We also generated an additional solution where the celestial and terrestrial pole offset corrections are modelled as stochastic parameters, using a random walk model, and evaluated the effect it has on EOP determination. We finally determined the effect of the different solutions on station position and baseline length repeatabilities.

Summary of Paper IV

We introduced a novel concept for the combination of co-located space geodetic installations which is called Combination Using a Single Point (CUSP). This concept treats two co-located stations as the origin and tip of the connecting vector between them. The station at the origin is used to estimate the variation of the location, i.e., translation of the origin. The station at the tip is used to estimate both the translation of the origin and the relative change of the tip, i.e., rotation/scale of the vector. The local tie measurements are used to estimate the rotation/scale of the vector. In order for this concept to have physical meaning, a significant degree of correlation between the station position variations of co-located

stations must exist. We studied whether co-located stations show this degree of correlation using the CONT17 dataset and concurrent GPS data of co-located GNSS stations. We devised our own metric to evaluate this effect and studied its statistical robustness using two-sample kolmogorov-smirnov tests. We evaluated what effect the COL with common troposphere between co-located VLBI and GPS stations has, with respect to station position variations, both when combining only zenith wet delays, and zenith wet delays and tropospheric gradients. We then performed a proof-of-concept study of the proposed CUSP method.

Summary of Paper V

We evaluated the tropospheric gradients from 4 different co-located GNSS stations comparing them to those obtained from a co-located water vapor radiometer. We used two different software packages, GipsyX and c5++, and employing the kalman filtering process we obtained time-series of tropospheric gradients over a period of 6 months. The study was done for three different elevation cutoff angles 5^o , 10^o and 20^o. Assuming that the radiometer estimates represent the ground truth, we assessed the performance of the GNSS stations, and saw whether differences can be attributed to the pillar installations and mounting methods employed in each one.

Bibliography

Aggrey, J. and S. Bisnath (2019). Improving GNSS PPP convergence: The case of atmospheric-constrained, multi-GNSS PPP-AR. *Sensors*, **19**(3), 587.

Agnew, D. C. (2015). Earth Tides. *Treatise on Geophysics, Volume 3: Geodesy*, 151–178. DOI: 10.1016/B978-0-444-53802-4.00058-0.

Altamimi, Z. and X. Collilieux (2009). IGS contribution to the ITRF. *Journal of Geodesy*, **83**(3-4), 375–383. DOI: 10.1007/s00190-008-0294-x.

Altamimi, Z., C. Boucher, and P. Sillard (2002). New trends for the realization of the International Terrestrial Reference System. *Advances in Space Research*, **30**(2), 175–184. DOI: 10.1016/S0273-1177(02)00282-X.

Altamimi, Z., X. Collilieux, and L. Métivier (2011). ITRF2008: an improved solution of the international terrestrial reference frame. *Journal of Geodesy*, **85**(8), 457–473. DOI: 10.1007/s00190-011-0444-4.

Altamimi, Z., P. Rebischung, L. Métivier, and X. Collilieux (2016). ITRF2014: A new release of the International Terrestrial Reference Frame modeling nonlinear station motions. *Journal of Geophysical Research: Solid Earth*, **121**(8), 6109–6131. DOI: 10.1002/2016JB013098.

Anderson, J. M., G. Beyerle, S. Glaser, L. Liu, B. Männel, T. Nilsson, R. Heinkelmann, and H. Schuh (2018). Simulations of VLBI observations of a geodetic satellite providing co-location in space. *Journal of Geodesy*, **92**(9), 1023–1046. DOI: 10.1007/s00190-018-1115-5.

Anderson, J. M. and M. H. Xu (2018). Source structure and measurement noise are as important as all other residual sources in geodetic VLBI combined. *Journal of Geophysical Research: Solid Earth*, **123**(11), 10–162.

Artz, T., L. Bernhard, A. Nothnagel, P. Steigenberger, and S. Tesmer (2012). Methodology for the combination of sub-daily Earth rotation from GPS and VLBI observations. *Journal of Geodesy*, **86**(3), 221–239. DOI: 0.1007/s00190-011-0512-9.

Artz, T., S. Halsig, A. Iddink, A. Nothnagel, and C. Tegtmeier (2016). "Constraining Least-Squares VLBI Solutions". *International VLBI Service for Geodesy and*

Astrometry 2016 General Meeting Proceedings: "New Horizons with VGOS". Ed. by D. Behrend, K. D. Baver, and K. L. Armstrong. NASA/CP-2016-219016, pp. 193–197.

Behrend, D., B. Petrachenko, C. Ruszczyk, and P. Elósegui (2019). "Roll-out status of the VGOS network". *poster, 24rd European VLBI group for geodesy and astrometry working meeting*.

Behrend, D., C. Thomas, J. Gipson, E. Himwich, and K. Le Bail (2020). On the organization of CONT17. *Journal of Geodesy*, **94**. DOI: 10.1007/s00190-020-01436-x.

Beutler, G., A. Villiger, R. Dach, A. Verdun, and A. Jäggi (2020). Long polar motion series: Facts and insights. *Advances in space research*, **66**(11), 2487–2515.

Biancale, R., D. Gambis, and R. J.-Y. (Oct. 2010). *Why combining at the Observation Level?* https://www.iers.org/SharedDocs/Publikationen/EN/IERS/WorkingGroups/CombinationOL/REFAG2010_Biancale.pdf?__blob=publicationFile&v=1.

Biggs, J., T. Wright, Z. Lu, and B. Parsons (2007). Multi-interferogram method for measuring interseismic deformation: Denali Fault, Alaska. *Geophysical Journal International*, **170**(3), 1165–1179. DOI: 10.1111/j.1365-246X.2007.03415.x.

Boehm, J., B. Werl, and H. Schuh (2006). Troposphere mapping functions for GPS and very long baseline interferometry from European Centre for Medium-Range Weather Forecasts operational analysis data. *Journal of Geophysical Research: Solid Earth*, **111**(B2). DOI: 10.1029/2005JB003629.

Böhm, J., T. Hobiger, R. Ichikawa, T. Kondo, Y. Koyama, A. Pany, H. Schuh, and K. Teke (2010). Asymmetric tropospheric delays from numerical weather models for UT1 determination from VLBI Intensive sessions on the baseline Wettzell–Tsukuba. *Journal of Geodesy*, **84**, 319–325.

Boucher, C., Z. Altamimi, P. Sillard, and M. Feissel-Vernier (2004). *The ITRF2000 (IERS Technical Note)*. Vol. 31. Frankfurt am Main: Verlag des Bundesamts für Kartographie und Geodäsie, pp. 1–289.

Boy, J.-P., J. Hinderer, and P. Gegout (1998). Global atmospheric loading and gravity. *Physics of the Earth and Planetary Interiors*, **109**(3-4), 161–177. DOI: 10.1016/S0031-9201(98)00122-8.

Brockmann, E., D. Ineichen, U. Marti, S. Schaer, A. Schlatter, and A. Villiger (July 2012). "Determination of Tectonic Movements in the Swiss Alps Using GNSS and Levelling". *International Association of Geodesy Symposia*. Vol. 136, pp. 689–695. DOI: 10.1007/978-3-642-20338-1_85.

Capitaine, N. (2008). "Nomenclature and numerical standards for IAU models and IERS Conventions for Earth rotation". *Proceedings of the Journées 2008 "Systèmes de référence spatio-temporels" & X. Lohrmann-Kolloquium: Astrome-*

try, Geodynamics and Astronomical Reference Systems. Ed. by M. Soffel and N. Capitaine. Lohrmann-Observatorium and Observatoire de Paris, pp. 46–49.

Cappallo, R. (2017). *FOURFIT user's manual*.

Charlot, P., C. Jacobs, D. Gordon, S. Lambert, A. de Witt, J. Böhm, A. Fey, R. Heinkelmann, E. Skurikhina, O. Titov, et al. (2020). The third realization of the International Celestial Reference Frame by very long baseline interferometry. *Astronomy & Astrophysics*. DOI: 10.1051/0004-6361/202038368.

Collins, P., F. Lahaye, P. Heroux, and S. Bisnath (2008). "Precise point positioning with ambiguity resolution using the decoupled clock model". *Proceedings of the 21st international technical meeting of the satellite division of the Institute of Navigation (ION GNSS 2008)*, pp. 1315–1322.

Dach, R., S. Schaer, S. Lutz, M. Meindl, H. Bock, E. Orliac, L. Prange, D. Thaller, L. Mervarta, A. Jäggi, G. Beutler, E. Brockmann, D. Ineichen, A. Wiget, G. Weber, H. Habrich, J. Ihde, P. Steigenberger, and U. Hugentobler (2013). "Center for Orbit Determination in Europe (CODE)". *International GNSS Service, Technical Report 2012 (IGS Annual Report)*. Ed. by R. Dach and Y. Jean. IGS Central Bureau and University of Bern, pp. 35–46. DOI: 10.7892/boris.80303.

Davis, J., T. Herring, I. Shapiro, A. Rogers, and G. Elgered (1985). Geodesy by radio interferometry: Effects of atmospheric modeling errors on estimates of baseline length. *Radio science*, **20**(6), 1593–1607. DOI: 10.1029/RS020i006p01593.

Diamantidis, P.-K. and R. Haas (2022). Evaluation of the first three years of VGOS 24 h sessions using a kalman filter with c5++. *Earth, Planets and Space*. in review.

Diamantidis, P.-K., R. Haas, and K. Le Bail (2023). On the possibility of site-based combinations using a single point. *Journal of Geodesy*. in review.

Diamantidis, P.-K., R. Haas, E. Varenius, M. Schartner, and S. Matsumoto (2022). Combining VGOS, legacy S/X and GNSS for the determination of UT1. *Journal of Geodesy*, **96**(8), 55. DOI: 10.1007/s00190-022-01648-3.

Diamantidis, P.-K., G. Kłopotek, and R. Haas (2021). VLBI and GPS inter-and intra-technique combinations on the observation level for evaluation of TRF and EOP. *Earth, Planets and Space*, **73**(1), 1–16. DOI: 10.1186/s40623-021-01389-1.

Ejigu, Y. G., A. Hunegnaw, K. E. Abraha, and F. N. Teferle (2019). Impact of GPS antenna phase center models on zenith wet delay and tropospheric gradients. *GPS Solutions*, **23**(1), 5. DOI: 10.1007/s10291-018-0796-9.

Elgered, G., T. Ning, P.-K. Diamantidis, and T. Nilsson (2023). Assessment of GNSS stations using atmospheric horizontal gradients and microwave radiometry. *Advances in Space Research*. in review.

Gambis, D., J.-Y. Richard, M. Seitz, and R. Biancale (2012). Combination of Space Geodetic Techniques at the Observation Level. *cosp*, **39**, 580.

Geng, J., X. Meng, A. H. Dodson, and F. N. Teferle (2010). Integer ambiguity resolution in precise point positioning: method comparison. *Journal of Geodesy*, **84**(9), 569–581. DOI: 10.1007/s00190-010-0399-x.

Gipson, J. (2010). "An introduction to Sked". *IVS 2010 General Meeting Proceedings "VLBI2010: From Vision to Reality"*. Ed. by D. Behrend and K. D. Baver. NASA/CP-2010-215864, pp. 77–84.

Griffiths, J. and J. R. Ray (2013). Sub-daily alias and draconitic errors in the IGS orbits. *GPS solutions*, **17**(3), 413–422.

Gurtner, W. and L. Estey (2007). Rinex-the receiver independent exchange format-version 3.00. *Astronomical Institute, University of Bern and UNAVCO, Bolulder, Colorado.*

Hearn, E., S. McClusky, S. Ergintav, and R. Reilinger (2009). Izmit earthquake post-seismic deformation and dynamics of the North Anatolian Fault Zone. *Journal of Geophysical Research: Solid Earth*, **114**(B8). DOI: 10.1029/2008JB006021.

Hernández-Pajares, M., J. Juan, J. Sanz, R. Orus, A. Garcia-Rigo, J. Feltens, A. Komjathy, S. Schaer, and A. Krankowski (2009). The IGS VTEC maps: a reliable source of ionospheric information since 1998. *Journal of Geodesy*, **83**(3-4), 263–275. DOI: 10.1007/s00190-008-0266-1.

Hobiger, T., T. Gotoh, T. Kubooka, M. Sekido, H. Takiguchi, and H. Takeuchi (2010). "c5++-multi-technique Analysis Software for Next Generation Geodetic Instruments". *IVS 2010 General Meeting Proceedings "VLBI2010: From Vision to Reality"*. Ed. by D. Behred and K. D. Baver. NASA/CP-2010-215864, pp. 212–216.

Hobiger, T. and T. Otsubo (2015). "Combination of space geodetic techniques on the observation level with c5++: common nuisance parameters and data weighting". *REFAG 2014. International Association of Geodesy Symposia*. Ed. by T. van Dam. Vol. 146. Springer, pp. 31–37. DOI: 10.1007/1345_2015_152.

Hobiger, T., C. Rieck, R. Haas, and Y. Koyama (2015). Combining GPS and VLBI for inter-continental frequency transfer. *Metrologia*, **52**(2), 251. DOI: 10.1088/0026-1394/52/2/251.

Jin, S., E. Cardellach, and F. Xie (2014). *GNSS Remote Sensing*. Springer. DOI: 10.1007/978-94-007-7482-7.

Johnston, G., A. Riddell, and G. Hausler (2017). "The International GNSS Service". *Springer Handbook of Global Navigation Satellite Systems*. Ed. by P. J. Teunissen and O. Montenbruck. Springer Handbooks. Springer, pp. 967–982. DOI: 10.1007/978-3-319-42928-1_33.

Klopotek, G., T. Hobiger, R. Haas, and T. Otsubo (2020). Geodetic VLBI for precise orbit determination of Earth satellites: a simulation study. *Journal of Geodesy*, **94**(6), 1–26.

Kondo, T. and K. Takefuji (2016). An algorithm of wideband bandwidth synthesis for geodetic VLBI. *Radio Science*, **51**(10), 1686–1702. DOI: 10.1002/2016RS006070.

Kotsakis, C. (Oct. 2018). "Datum Definition and Minimal Constraints". *Encyclopedia of Geodesy. Encyclopedia of Earth Sciences Series.* Ed. by E. Grafarend. Springer. DOI: 10.1007/978-3-319-02370-0_157-1.

Kouba, J. (2009). *A guide to using International GNSS Service (IGS) products.* http://acc.igs.org/UsingIGSProductsVer21.pdf.

Krügel, M., D. Thaller, V. Tesmer, M. Rothacher, D. Angermann, and R. Schmid (2007). Tropospheric parameters: combination studies based on homogeneous VLBI and GPS data. *Journal of Geodesy*, **81**(6-8), 515–527. DOI: 10.1007/s00190-006-0127-8.

Kumar, S. and K. B. Moore (2002). The Evolution of Global Positioning System (GPS) Technology. *Journal of Science Education and Technology*, **11**(1), 59–80. DOI: 10.1023/A:1013999415003.

Landskron, D. and J. Böhm (2018). VMF3/GPT3: refined discrete and empirical troposphere mapping functions. *Journal of Geodesy*, **92**(4), 349–360. DOI: 10.1007/s00190-017-1066-2.

— (2019). Improving dUT1 from VLBI intensive sessions with GRAD gradients and ray-traced delays. *Advances in Space Research*, **63**(11), 3429–3435.

Laurichesse, D., F. Mercier, J.-P. Berthias, P. Broca, and L. Cerri (2009). Integer Ambiguity Resolution on Undifferenced GPS Phase Measurements and its Application to PPP and Satellite Precise Orbit Determination. *Navigation*, **56**(2), 135–149. DOI: 10.1002/j.2161-4296.2009.tb01750.x.

MacMillan, D., D. Behrend, and S. Kurihara (2012). "Effects of the 2011 Tohoku earthquake on VLBI geodetic measurements". *Proceedings 7th International VLBI Service for geodesy and astrometry 2012 General Meeting*, pp. 440–444.

MacMillan, D., A. Fey, J. Gipson, D. Gordon, C. Jacobs, H. Krásná, S. Lambert, Z. Malkin, O. Titov, G. Wang, et al. (2019). Galactocentric acceleration in VLBI analysis-Findings of IVS WG8. *Astronomy & Astrophysics*, **630**, A93.

Malkin, Z. (2009). On comparison of the Earth orientation parameters obtained from different VLBI networks and observing programs. *Journal of Geodesy*, **83**(6), 547–556. DOI: 10.1007/s00190-011-0483-x.

Miller, S. and C. Wunsch (1973). The pole tide. *Nature Physical Science*, **246**(155), 98–102. DOI: 10.1038/physci246098a0.

Montenbruck, O., P. Steigenberger, L. Prange, Z. Deng, Q. Zhao, F. Perosanz, I. Romero, C. Noll, A. Stürze, G. Weber, R. Schmid, K. MacLeod, and S. Schaer (2017). The Multi-GNSS Experiment (MGEX) of the International GNSS Service (IGS) – Achievements, prospects and challenges. *Advances in Space Research*, **59**(7), 1671–1697. DOI: 10.1016/j.asr.2017.01.011.

Noll, C. E. (2010). The crustal dynamics data information system: A resource to support scientific analysis using space geodesy. *Advances in Space Research*, **45**(12), 1421–1440. DOI: 10.1016/j.asr.2010.01.018.

Nothnagel, A., T. Artz, D. Behrend, and Z. Malkin (2017). International VLBI service for geodesy and astrometry. *Journal of Geodesy*, **91**(7), 711–721.

Nothnagel, A., C. Holst, and R. Haas (2019). A VLBI delay model for gravitational deformations of the Onsala 20 m radio telescope and the impact on its global coordinates. *Journal of Geodesy*, **93**(10). DOI: 10.1007/s00190-019-01299-x.

Nothnagel, A. (2009). Conventions on thermal expansion modelling of radio telescopes for geodetic and astrometric VLBI. *Journal of Geodesy*, **83**(8), 787–792. DOI: 10.1007/s00190-008-0284-z.

Petit, G., F. Arias, and G. Panfilo (2015). International atomic time: Status and future challenges. *Comptes Rendus Physique*, **16**(5), 480–488.

Petit, G. and B. Luzum (2010). *IERS Conventions (2010) (IERS Technical Note)*. Vol. 36. Frankfurt am Main: Verlag des Bundesamts für Kartographie und Geodäsie, pp. 1–179.

Petrachenko, B., A. Niell, D. Behrend, B. Corey, J. Böhm, P. Chralot, A. Collioud, J. Gipson, R. Haas, T. Hobiger, et al. (2009). *Design aspects of the VLBI2010 system-Progress report of the IVS VLBI2010 committee*. Tech. rep.

Prange, L., R. Dach, S. Lutz, S. Schaer, and A. Jäggi (2016). "The CODE MGEX orbit and clock solution". *IAG 150 Years: Proceedings of the IAG Scientific Assembly in Postdam, Germany, 2013*. Springer, pp. 767–773.

Prange, L., E. Orliac, R. Dach, D. Arnold, G. Beutler, S. Schaer, and A. Jäggi (2017). CODE's five-system orbit and clock solution—the challenges of multi-GNSS data analysis. *Journal of Geodesy*, **91**(4), 345–360. DOI: 10.1007/s00190-016-0968-8.

Preston, R. A., D. Morabito, A. Wehrle, D. Jauncey, M. Batty, R. Haynes, A. Wright, and G. Nicolson (1983). VLBI observations of a radio flare of Circinus X-1. *The Astrophysical Journal*, **268**, L23–L26. DOI: 10.1086/184022.

Ray, J. and Z. Altamimi (2005). Evaluation of co-location ties relating the VLBI and GPS reference frames. *Journal of Geodesy*, **79**(4-5), 189–195. DOI: 10.1007/s00190-005-0456-z.

Rothacher, M., G. Beutler, D. Behrend, A. Donnellan, J. Hinderer, C. Ma, C. Noll, J. Oberst, M. Pearlman, H.-P. Plag, et al. (2009). "The future global geodetic

observing system". *Global Geodetic Observing System: Meeting the Requirements of a Global Society on a Changing Planet in 2020*. Springer, pp. 237–272.

Rothacher, M., G. Beutler, T. A. Herring, and R. Weber (1999). Estimation of nutation using the Global Positioning System. *Journal of Geophysical Research: Solid Earth*, **104**(B3), 4835–4859. DOI: 10.1029/1998JB900078.

Schartner, M. and J. Böhm (2019). VieSched++: a New VLBI Scheduling Software for Geodesy and Astrometry. *Publications of the Astronomical Society of the Pacific*, **131**(1002), 084501. DOI: 10.1088/1538-3873/ab1820.

Scherneck, H.-G. and F. H. Webb (1999). "Ocean tide loading and diurnal tidal motion of the solid Earth centre". *IERS Analysis Campaign to Investigate Motions of the Geocenter (IERS Technical Note 25)*. Ed. by J. Ray. Central Bureau of IERS - Observatoire de Paris, pp. 85–91.

Shaffer, D. B. (2000). "RFI: Effects on Bandwidth Synthesis". *International VLBI Service for Geodesy and Astrometry 2000 General Meeting Proceedings*. Ed. by N. Vandenberg and K. D. Baver. NASA/CP-2000-209893, pp. 402–406.

Sillard, P. and C. Boucher (2001). A review of algebraic constraints in terrestrial reference frame datum definition. *Journal of Geodesy*, **75**(2-3), 63–73.

Sovers, O. J., J. L. Fanselow, and C. S. Jacobs (1998). Astrometry and geodesy with radio interferometry: experiments, models, results. *Reviews of Modern Physics*, **70**(4), 1393. DOI: 10.1103/RevModPhys.70.1393.

Springer, T., F. Dilssner, D. Escobar, C. Flohrer, O. Otten, D. Svehla, and R. Zandbergen (2011). NAPEOS: The ESA/ESOC tool for Space Geodesy. *Geophysical Research Abstracts*, **13**. EGU2011-8287.

Teke, K., J. Böhm, M. Madzak, Y. Kwak, and P. Steigenberger (2015). GNSS zenith delays and gradients in the analysis of VLBI Intensive sessions. *Advances in Space Research*, **56**(8), 1667–1676.

Teunissen, P., P. Joosten, and C. Tiberius (2002). "A comparison of TCAR, CIR and LAMBDA GNSS ambiguity resolution". *Proceedings of the 15th International Technical Meeting of the Satellite Division of the Institute of Navigation (ION GPS 2002)*, pp. 2799–2808.

Thaller, D. (2008). "Inter-technique combination based on homogeneous normal equation systems including station coordinates, Earth orientation and troposphere parameters". PhD thesis. Technische Universität München.

Thaller, D., R. Dach, M. Seitz, G. Beutler, M. Mareyen, and B. Richter (2011). Combination of GNSS and SLR observations using satellite co-locations. *Journal of Geodesy*, **85**(5), 257–272. DOI: 10.1007/s00190-010-0433-z.

Tsiforos, N. (1975). *Greek Mythology*. translation by P.-K. Diamantidis, p. 10.

Walpersdorf, A., E. Calais, J. Haase, L. Eymard, M. Desbois, and H. Vedel (2001). Atmospheric gradients estimated by GPS compared to a high resolution nu-

merical weather prediction (NWP) model. *Physics and Chemistry of the Earth, Part A: Solid Earth and Geodesy*, **26**(3), 147–152. DOI: 10.1016/S1464-1895(01)00038-2.

Wang, J., M. Ge, S. Glaser, K. Balidakis, R. Heinkelmann, and H. Schuh (2022a). Impact of Tropospheric Ties on UT1-UTC in GNSS and VLBI Integrated Solution of Intensive Sessions. *Journal of Geophysical Research: Solid Earth*, **127**(11), e2022JB025228.

— (2022b). Improving VLBI analysis by tropospheric ties in GNSS and VLBI integrated processing. *Journal of Geodesy*, **96**(4), 32.

Whitney, A., A. Rogers, H. Hinteregger, C. Knight, J. Levine, S. Lippincott, T. Clark, I. Shapiro, and D. Robertson (1976). A very-long-baseline interferometer system for geodetic applications. *Radio Science*, **11**(5), 421–432. DOI: 10.1029/RS011i005p00421.

Williams, S. and N. Penna (2011). Non-tidal ocean loading effects on geodetic GPS heights. *Geophysical Research Letters*, **38**(9). DOI: 10.1029/2011GL046940.

Wresnik, J., R. Haas, J. Boehm, and H. Schuh (2007). Modeling thermal deformation of VLBI antennas with a new temperature model. *Journal of Geodesy*, **81**(6-8), 423–431. DOI: 10.1007/s00190-006-0120-2.

Xia, F., S. Ye, P. Xia, L. Zhao, N. Jiang, D. Chen, and G. Hu (2019). Assessing the latest performance of Galileo-only PPP and the contribution of Galileo to Multi-GNSS PPP. *Advances in space research*, **63**(9), 2784–2795.

Zumberge, J. and G. Gendt (2001). The demise of selective availability and implications for the international GPS service. *Physics and Chemistry of the Earth, Part A: Solid Earth and Geodesy*, **26**(6-8), 637–644.